SMRT | A WORLD OF KNOWLEDGE
FOR MR TECHNOLOGISTS & RADIOGRAPHERS

SECTION FOR MAGNETIC RESONANCE TECHNOLOGISTS
OF THE INTERNATIONAL SOCIETY FOR MAGNETIC RESONANCE IN MEDICINE

Home Studies Educational Seminars

VOLUME 16 • NUMBER 4

MR Angiography: Technical Considerations & Developments

Technical Considerations in MR Angiography: An Image-Based Guide

John N. Morelli, M.D.
Clint M. Gerdes, M.D.
Peter Schmitt, Ph.D.
Tao Ai, M.D.
Megan R. Saettele, M.D.
Val M. Runge, M.D.
Ulrike I. Attenberger, M.D.

Non-Contrast Enhanced MR Angiography: Physical Principles

Andrew J. Wheaton, Ph.D.
Mitsue Miyazaki, Ph.D.

Editor, SMRT Educational Seminars, Home Study Program

Anne Marie Sawyer, B.S., R.T.(R)(MR), FSMRT
Home Study Program
Lucas Center for Imaging
Stanford University, Stanford, California, USA
T: +1 650 725 9697
E: amsawyer@stanford.edu

Chair, SMRT Publications Committee

Vanessa Orchard, DCR (R), PGDip.(Nuc Med), M.Sc.(MRI)
Lead Radiographer
Cardiac Imaging Centre
Golden Jubilee National Hospital
Dunbartonshire, Glasgow, Scotland, UK
T: +0141 951 5187
E: vanessa.orchard@gjnh.scot.nhs.uk

MR Angiography: Technical Considerations & Developments

December 2013

We are pleased to present the SMRT Educational Seminars, Volume 16, Number 4: "MR Angiography: Technical Considerations & Developments." This is the 62nd accredited home study developed by the SMRT, exclusively for SMRT members. The accreditation is conducted by the SMRT acting as a RCEEM (Recognized Continuing Education Evaluation Mechanism) for the ARRT. Category A credits are assigned to each home study, which can be used to maintain one's ARRT advanced registry. SMRT Home Studies are also approved for AIR (Australian Institute of Radiography), NZIMRT (New Zealand Institute of Radiation Technology) and CPD Now (The College of Radiographers, United Kingdom) continuing professional development (CPD) activities.

Two peer-reviewed articles have been chosen for this home study issue. The authors of the first, "Technical Considerations in MR Angiography: An Image-Based Guide," introduce their article by saying, "As the complexity of the magnetic resonance angiography (MRA) techniques grows, it becomes more difficult . . . to appreciate the physical principles underlying these studies. Nevertheless, such an understanding is requisite for improving clinical image quality." In addition, " . . . a general understanding of technical factors influencing MRA can improve image quality in day-to-day practice, ultimately affecting patient care through the production of clinical images more optimally tailored to answer the specific clinical question at hand."

"As the complexity of the magnetic resonance angiography (MRA) techniques grows, it becomes more difficult . . . to appreciate the physical principles underlying these studies. Nevertheless, such an understanding is requisite for improving clinical image quality.

In the second article, "Non-Contrast-Enhanced MR Angiography: Physical Principles," the authors review the original non-contrast enhanced techniques and the more recently developed. They state "Advances in hardware and software have made NCE-MRA scan time clinically feasible. Recent concerns over the safety of gadolinium-based contrast material combined with the expense of the material and its administration have generated a demand for NCE-MRA."

A special thank you to Anna Simeonov from Toronto, Quebec, Canada for acting as the Expert Reviewer.

Thanks also to Heidi Berns, M.S., R.T.(R)(MR), FSMRT, Chair of the SMRT RCEEM Ad-hoc committee from Coralville, Iowa, USA and all those who participate on this committee by reviewing the home studies for accreditation. Finally, many thanks to Jennifer Olson, Associate Executive Director, Mary Keydash, Publications Director, Linda O-Brown, SMRT Coordinator, Sally Moran, Director of Electronic Communications and the entire staff in the Berkeley, California, USA office of the ISMRM and SMRT for their insight and long hours spent supporting these educational symposia.

MR Angiography: Technical Considerations & Developments

SECTION FOR MAGNETIC RESONANCE TECHNOLOGISTS

Home Studies *Educational Seminars*

VOLUME 16 • NUMBER 4

Educational Objectives

Technical Considerations in MR Angiography: An Image-Based Guide

- Review Time-of-Flight principles including flow effects, 2D and 3D acquisition schemes, flip angle and TR effects, field strength effects and magnetization transfer; and show image examples;
- Describe Phase-Contrast MRA including flow-encoding gradients; and show image examples;
- Discuss Contrast-Enhanced MRA including bolus arrival and K-space, post-processing, dose reduction techniques; and show image examples;
- Explain Nephrogenic Systemic Fibrosis (NSF), relaxivity of contrast media, and protein-binding agents; and
- Describe parallel imaging techniques at 3T, dynamic imaging and balanced steady-state free precession; and show image examples.

Non-Contrast Enhanced MR Angiography: Physical Principles

- Review the history of MR angiography techniques, non-contrast and contrast-enhanced methods.
- Describe inflow-based techniques including the general mechanism and limitations, 3D TOF, HOP-MRA, 2D TOF, and QISS; and show image examples;
- Discuss cardiac phase-dependent techniques including the general mechanism, and cardiac-gated 3D Fast-Spin-Echo NCE-MRA; and show image examples;
- Explain flow-encoding techniques including the general mechanism, conventional phase contrast, 4D Flow, and flow-sensitive dephasing; and show image examples;
- Review spin-labeling techniques including the general mechanism, Flow-In Spin Labeling, Flow-Out Spin Labeling, Tag-Alternation Spin Labeling; and show image examples; and
- Describe relaxation-based techniques including the general mechanism and bSSFP.

Expert Reviewer

Anna Simeonov, MSc, MRT (MR)(R)
Senior MRI Technologist
Princess Margaret Cancer Center, Toronto
Lecturer, Radiation Medicine Program
University of Toronto
Toronto, Ontario, Canada

Technical Considerations in MR Angiography: An Image-Based Guide

John N. Morelli, M.D.,[1] Clint M. Gerdes, M.D.,[1] Peter Schmitt, Ph.D.,[2] Tao Ai, M.D.,[3]*
Megan R. Saettele, M.D.,[4] Val M. Runge, M.D.,[5] and Ulrike I. Attenberger, M.D.[6]

Reprinted with permission from the ISMRM Journal of Magnetic Resonance Imaging: Volume 37: Pages 1326 - 1341, (C) 2013 with permission from Wiley-Liss, Inc.

This article is accredited as a journal-based CME activity. If you wish to receive credit for this activity, please refer to the website: www.wileyhealthlearning.com

ACCREDITATION AND DESIGNATION STATEMENT

Blackwell Futura Media Services designates this journal-based CME activity for a maximum of 1 *AMA PRA Category 1 Credit*™. Physicians should only claim credit commensurate with the extent of their participation in the activity.

Blackwell Futura Media Services is accredited by the Accreditation Council for Continuing Medical Education to provide continuing medical education for physicians.

EDUCATIONAL OBJECTIVES

Upon completion of this educational activity, participants will be better able to list the variety of MR angiographic (MRA) techniques available, describe simple ways to modify sequence parameters to improve image quality and reduce contrast dose, and explain the physical principles behind newer MRA techniques.

ACTIVITY DISCLOSURES

No commercial support has been accepted related to the development or publication of this activity.

Faculty Disclosures:

Editor-in-Chief: C. Leon Partain, MD, PhD has no conflicts of interest to disclose.

CME Editor: Scott B. Reeder, MD, PhD has no conflicts of interest to disclose.

CME Committee: Pratik Mukherjee, MD, PhD, Shreyas Vasanawala, MD, PhD, Bonnie Joe, MD, PhD, Tim Leiner, MD, PhD, Sabine Weckbach, MD, and Frank Korosec, PhD have no conflicts of interest to disclose. Scott K. Nagle, MD, PhD discloses a personal shareholder investment in GE. Mustafa R. Bashir, MD discloses research support from Bracco Diagnostics and Siemens Healthcare, and consultant honorarium from Bayer Pharmaceuticals.

Authors: John N. Morelli, MD, Clint M. Gerdes, MD, Peter Schmitt, PhD, Tao Ai, MD, Megan R. Saettele, MD, Val M. Runge, MD, and Ulrike I. Attenberger, MD have no conflicts of interest to disclose.

This manuscript underwent peer review in line with the standards of editorial integrity and publication ethics maintained by *Journal of Magnetic Resonance Imaging*. The peer reviewers have no relevant financial relationships. The peer review process for *Journal of Magnetic Resonance Imaging* is double-blinded. As such, the identities of the reviewers are not disclosed in line with the standard accepted practices of medical journal peer review.

Conflicts of interest have been identified and resolved in accordance with Blackwell Futura Media Services's Policy on Activity Disclosure and Conflict of Interest. No relevant financial relationships exist for any individual in control of the content and therefore there were no conflicts to resolve.

INSTRUCTIONS ON RECEIVING CREDIT

For information on applicability and acceptance of CME credit for this activity, please consult your professional licensing board.

This activity is designed to be completed within an hour; physicians should claim only those credits that reflect the time actually spent in the activity. To successfully earn credit, participants must complete the activity during the valid credit period.

Follow these steps to earn credit:

- Log on to www.wileyhealthlearning.com
- Read the target audience, educational objectives, and activity disclosures.
- Read the article in print or online format.
- Reflect on the article.
- Access the CME Exam, and choose the best answer to each question.
- Complete the required evaluation component of the activity.

This activity will be available for CME credit for twelve months following its publication date. At that time, it will be reviewed and potentially updated and extended for an additional period.

[1]Department of Radiology, Scott & White Clinic and Hospital, Texas A&M University Health Science Center, Temple, Texas, USA
[2]Siemens Healthcare Erlangen, Bavaria, Germany
[3]Department of Radiology, Tongji Hospital, Tongji Medical College, Hua Zhong University of Science and Technology, WuHan, China
[4]Department of Radiology, University of Missouri-Kansas City, Saint Luke's Hospital, Kansas City, Missouri, USA
[5]Department of Radiology, University of Texas Medical Branch, Galveston, Texas, USA

As the complexity of the magnetic resonance angiography (MRA) techniques grows, it becomes more difficult for the practicing radiologist to appreciate the physical principles underlying these studies. Nevertheless, such an understanding is requisite for improving clinical image quality. As radiologists are most accustomed to dealing with medical images in everyday practice, it seems natural that an image-based approach to teaching MRA physics, rather than complex mathematical equations or pulse sequence diagrams, would be preferable. This article adopts such an approach. Simple ways to improve MRA image quality are emphasized along with new technologies and their physical basis. The ultimate goal of the article is to facilitate the practicing radiologist becoming more aware of the variety of MR techniques available, being more confident in modifying sequence parameters to improve image quality and reduce contrast dose, and understanding the basis behind newer MRA techniques.

Keywords: magnetic resonance angiography; magnetic resonance venography; gadolinium chelates; parallel imaging; 3 T
J. Magn. Reson. Imaging 2013;37:1326–1341.

THE PITFALLS OF CONVENTIONAL catheter-based x-ray angiography are well known and include its invasive nature, exposure to ionizing radiation, relative expense, and utilization of potentially nephrotoxic contrast media. While conventional angiography remains the clinical gold standard for diagnosis, magnetic resonance angiography (MRA) has become the noninvasive modality of choice (1–4) for many diagnoses. MRA is frequently used as a prerequisite to catheter angiography for planning purposes, even when intervention is certain.

Like most clinical MRI, innovations in MRA have been driven primarily by advances in hardware. Early MRA techniques included time-of-flight (TOF) and phase-contrast imaging. Continued improvements in MR hardware, including the ability to markedly reduce acquisition time, have brought contrast-enhanced MRA to the forefront. Mobile examination tables allowed multiple stations to be imaged following a single dose of gadolinium chelate. More recently, greater field strengths and the advent of parallel imaging have markedly reduced acquisition times for contrast-enhanced MRA, resulting in gains of both spatial and temporal resolution. Since the recently established link between nephrogenic systemic fibrosis and certain gadolinium contrast agents, the aforementioned innovations have also been explored to provide reductions in gadolinium chelate dose not only in MRA but in other MR applications as well (3,5,6). While all methods mentioned up to now are typically based on gradient-echo acquisition, newer noncontrast techniques have become increasingly popular, which use other types of sequences such as balanced steady-state free precession (b-SSFP) (7).

While understanding the underlying physics of MRA is not the primary duty of the practicing radiologist, a general understanding of technical factors influencing MRA image quality can improve image quality in day-to-day practice, ultimately affecting patient care through the production of clinical images more optimally tailored to answer the specific clinical question at hand. Understanding potential artifacts and shortcomings of MRA techniques can likewise aid in image interpretation. The present work aims to present the technical considerations of MRA in a context familiar to most radiologists—clinical images.

TIME-OF-FLIGHT

Flow Effects

In principle, both spin echo and gradient echo sequences are capable of depicting flow within vascular structures. In the case of the former, however, flowing protons typically encounter significant dephasing effects, which can lead to flow voids and image artifacts. In 2D spin echo imaging, if vessels are oriented relatively perpendicular to the imaging plane the blood might not persist within the imaged volume long enough to be subjected to both the 90° and 180° radiofrequency (RF) pulses. As such, at the time of readout (ie, echo time or TE), blood within the vascular structures demonstrates no signal.

Hence, gradient echo sequences were used to depict the arterial vasculature with high signal intensity. The advantages of gradient echo techniques include shorter echo times and no additional 180° rephrasing RF pulse. However, the latter characteristic renders these sequences more prone to susceptibility artifacts. Figure 1 demonstrates an example of flow-related enhancement. "Fresh" blood which has not been previously saturated by exposure to RF pulses replenishes the blood within the imaging volume that has been exposed to the previous RF pulse. These new unsaturated protons enter the imaging volume carrying their full longitudinal magnetization which can then be converted to transverse magnetization and subsequent high image signal intensity. Thus, at readout, blood within the arteries is likely to contain more protons with a greater net longitudinal magnetization than the stationary tissues, since protons within the stationary tissues have not fully recovered their longitudinal magnetization from the initial excitation pulse. When repetition times (TR) are sufficiently short, stationary protons may retain residual transverse magnetization due to the TE being much shorter than the T2 and T2* decay rates. Such residual transverse magnetization

[6]Institute of Clinical Radiology and Nuclear Medicine, University Medical Center Mannheim, University of Heidelberg, Mannheim, Germany
The first two authors contributed equally to this work.
*Address reprint requests to: T.A., Department of Radiology, Tongji Hospital, Tongji Medical College, Huazhong University of Science and Technology, Wuhan, China. E-mail: aitao007@hotmail.com
Received May 26, 2012; Accepted March 20, 2013
DOI 10.1002/jmri.24174
View this article online at wileyonlinelibrary.com.

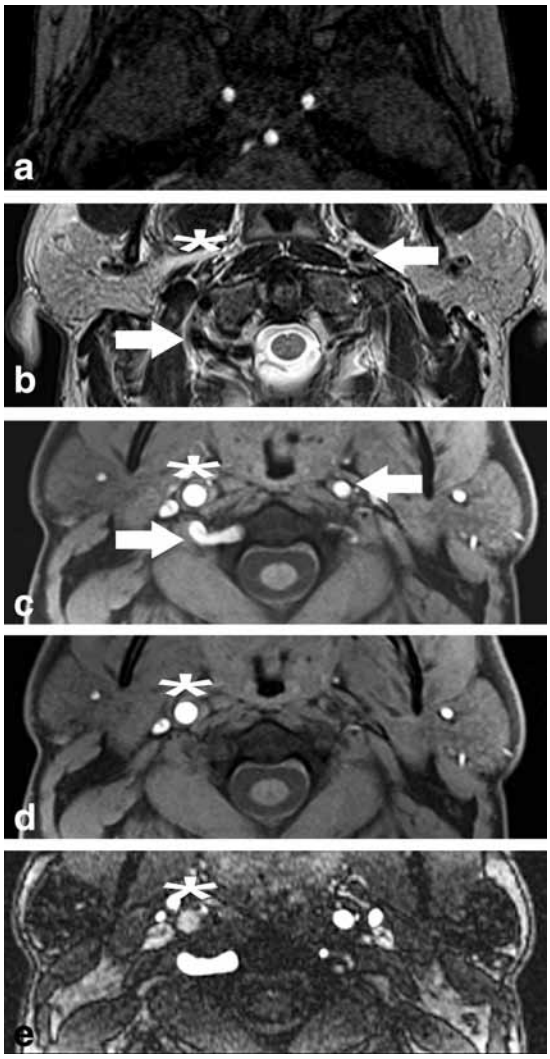

Figure 1. Axial (**a**) 3D TOF in a normal patient and (**b**) T2, (**c**) 3D TOF without and (**d**) with an inferiorly placed spatial saturation pulse, and (**e**) contrast-enhanced MRA images in a patient with a right carotid occlusion. All noncontrast images were acquired with a superiorly placed saturation band to suppress venous signal. Normal bilateral internal carotid and vertebral artery (the right vertebral artery is dominant) signal intensity is seen in the (a) normal patient. Normal flow voids are seen in the right vertebral and left carotid (white arrows) arteries on the (b) T2-weighted images with corresponding high intravascular signal demonstrated in these areas on the (c) TOF images in the patient with a right carotid occlusion. On the (c) TOF images, the high signal within the right internal carotid artery (asterisk) could easily be mistaken for normal intravascular flow. The right internal carotid artery flow void is absent (asterisk) on the (b) T2-weighted image. With application of an additional (c) inferiorly placed spatial saturation pulse, there is drop-out of intravascular signal in the left carotid and bilateral vertebral arteries with persistent high signal within the occluded right internal carotid artery (asterisk). This high signal is due to the short T1 of deoxyhemoglobin found in thrombus. On the contrast-enhanced images, this thrombus is demonstrated as relative hypointensity relative to the enhancing left carotid artery.

can efficiently be eliminated (ie, spoiled) by application of appropriate gradient schemes and phase cycles of the excitation RF pulses. Spoiled gradient echo sequences are the main technique used for TOF MRA. Contrast on TOF images is T1-weighted with the degree of such weighting dependent on TR and the flip angle.

2D Time-of-Flight

2D TOF MRA consists of imaging multiple thin slices sequentially. As discussed above, short TRs limit the longitudinal magnetization recovery that can occur within in-slice stationary tissue, thus accentuating signal from flowing protons within the vasculature possessing minimally saturated longitudinal magnetization. Selective spatial saturation pulses that affect in-flowing protons can be used to suppress arterial or venous signal depending on their placement. Pitfalls include tissues with an intrinsic rapid T1 recovery such as methemoglobin and fat which may result in high signal due to T1 effects, as opposed to angiographic effects. This is also a potential pitfall for 3D TOF as illustrated in Fig. 1. Additionally, saturation effects can occur in longitudinally oriented vessels, limiting the evaluation.

2D vs. 3D Time-of-Flight

2D TOF techniques for MRA can artifactually make a given stenosis appear more severe. This is illustrated in Fig. 2. This exaggeration is secondary to motion-induced dephasing effects from turbulent flow. Relative to 2D TOF sequences, 3D acquisitions use shorter TE and have smaller voxel sizes, minimizing intravoxel dephasing (signal losses from phase incoherence), thus decreasing such flow-related signal loss (8). For these reasons, contrast-enhanced techniques have replaced 2D TOF for imaging of the cervical carotid vasculature, whereas 3D TOF is preferred for imaging of the Circle of Willis secondary to its isotropic resolution. The long scan time of 2D TOF sequences are a further disadvantage, although the technique is still occasionally used for intracranial venography.

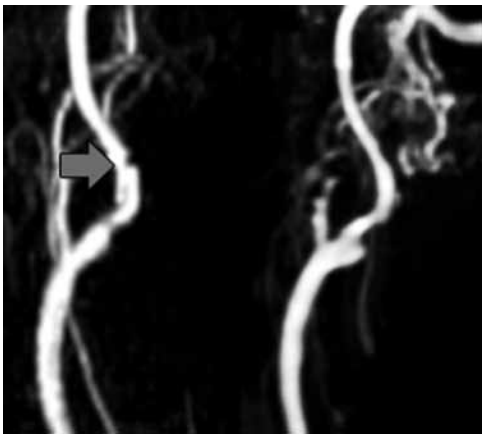

Figure 2. Sagittal MIP noncontrast TOF (left) and contrast-enhanced (right) and noncontrast TOF (right) MRA performed sequentially both demonstrate a focal, greater than 50% stenosis of the internal carotid artery at its origin. A less than 50% stenosis is present distally within the internal carotid artery on the (right) contrast-enhanced images; however, the degree of stenosis is artifactually accentuated on the (left, gray arrow) TOF images.

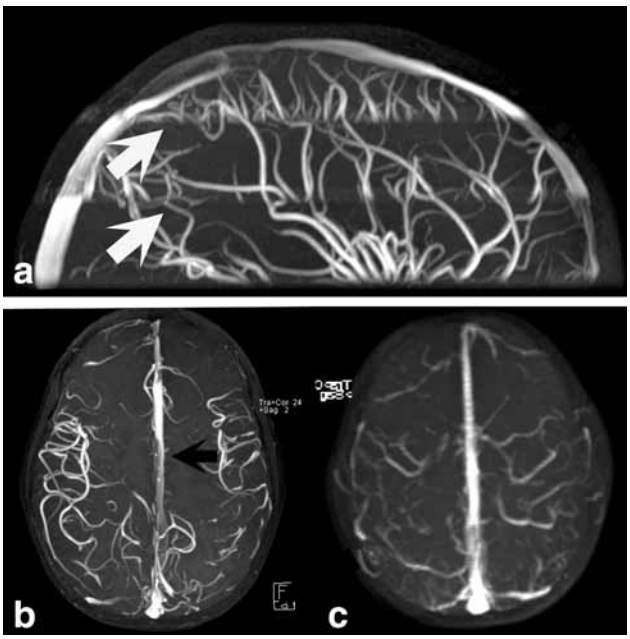

Figure 3. MIPs from (**a**,**b**) 3D TOF and (**c**) 2D TOF imaging of the high cerebral vasculature are shown. While 2D images are obtained in slices, 3D images are obtained in volumes or slabs. Multiple slabs are typically used for clinical 3D TOF imaging as shown in (a) (white arrows), with band-like artifacts denoting slab junctions. The (b) axial 3D TOF image also depicts the small, high cerebral arteries more clearly than the (c) 2D TOF technique due to greater SNR and spatial resolution. The improved vascular detail was useful in this particular patient: a relative paucity of high cerebral vasculature was present on the left side of the brain (b), findings consistent with the patient's known diagnosis of Moyamoya. The appearance of the sagittal venous sinus (black arrow) on the 3D images is due to flow saturation effects.

2D TOF images are typically displayed in maximum intensity projection (MIP) format, whereby images are "stacked" in order to produce the angiographic type image most familiar to radiologists, as shown in Fig. 2. While such projections are helpful to visualize vascular anatomy and pathology, source images must also be reviewed to evaluate extravascular tissues excluded from view on MIP images and to assess motion artifacts and artifactual signal loss (ie, signal loss due to susceptibility artifacts) (9,10). 3D TOF angiography is optimally obtained with isotropic voxel sizes, allowing multiplanar reconstructions to be performed in any desired imaging plane. While 2D images are obtained in slices, 3D images are obtained in volumes or slabs (11). Acquisition of 3D scans utilizing one large slab is disadvantageous due to saturation effects, a result of blood protons remaining in the image volume longer and thus being exposed to multiple RF pulses, thus decreasing signal (12). As a compromise between 2D and thick-slab 3D techniques, multiple slabs are typically used for clinical 3D TOF imaging with band-like artifacts often denoting slab junctions. With this traditional multislab technique, there is potential for signal starvation secondary to in-plane or "in-slab" flow. This is illustrated in Fig. 3.

Flip Angle and TR

As mentioned previously, image quality in TOF MRA is dependent on the difference in signal between moving and stationary tissues, rendering suppression of signal from the latter paramount. Maintaining this signal difference is more difficult with 3D TOF techniques, as imaging of blood flow occurs over a large slab rather than within a thin slice: in 3D acquisitions, blood remains within the imaged volume longer and may be subject to multiple RF pulses. The effects of such RF pulses are primarily dependent on the flip angle and TR. The result of flip angle variations is illustrated in Fig. 4a,b. High flip angles result in greater saturation of background tissue but also predispose flowing protons to saturation effects. Low flip angles result in the opposite. Adjustments in TR have analogous effects: longer TRs reduce background suppression while minimizing saturation effects, whereas shorter TRs maximize background suppression and saturation effects on flowing protons. Thus, longer TRs and smaller flip angles improve vessel conspicuity farther into the slab but decrease vessel conspicuity at the point of entry. To minimize saturation effects on the flowing blood, flip angles may also be varied across the imaging slab (13).

Field Strength Effects

Imaging at greater field strengths has been shown to be advantageous for TOF MRA (14). One reason is that the T1 of most structures constituting "background" tissue for TOF MRA is longer at 3 T (and progressively greater at 7 T) than at 1.5 T, leading to less background signal for a given TR due to slower recovery of longitudinal magnetization. Like the background tissues, the T1 of blood also increases at 3 T relative to 1.5 T. The increase in T1 does not affect signal of the inflowing blood, as incoming blood protons possess minimally saturated longitudinal magnetization and are not as directly dependent on longitudinal recovery rates for their signal in the image. Improvements in intravascular signal relative to background at higher filed strengths can be used as a type of currency and exchanged for reductions in scan time (ie, through parallel imaging) or increases in spatial resolution. Additionally, lower flip angles may be used to preserve penetration depth at higher field strength.

Magnetization Transfer

The concept of magnetization transfer requires an understanding of the main pools of body tissue protons—the free and bound pool. Free protons typically contribute to signal; protons in the bound pool are closely associated with macromolecules and have T2 times too short for detection. These two pools are coupled, allowing spin states of protons in the bound pool to influence those in the mobile pool. Saturation of protons in the bound pool, which have greater sensitivity to off-resonance RF pulses, can thus be transferred to protons in the mobile pool (15). This results in suppression of signal from soft tissue structures

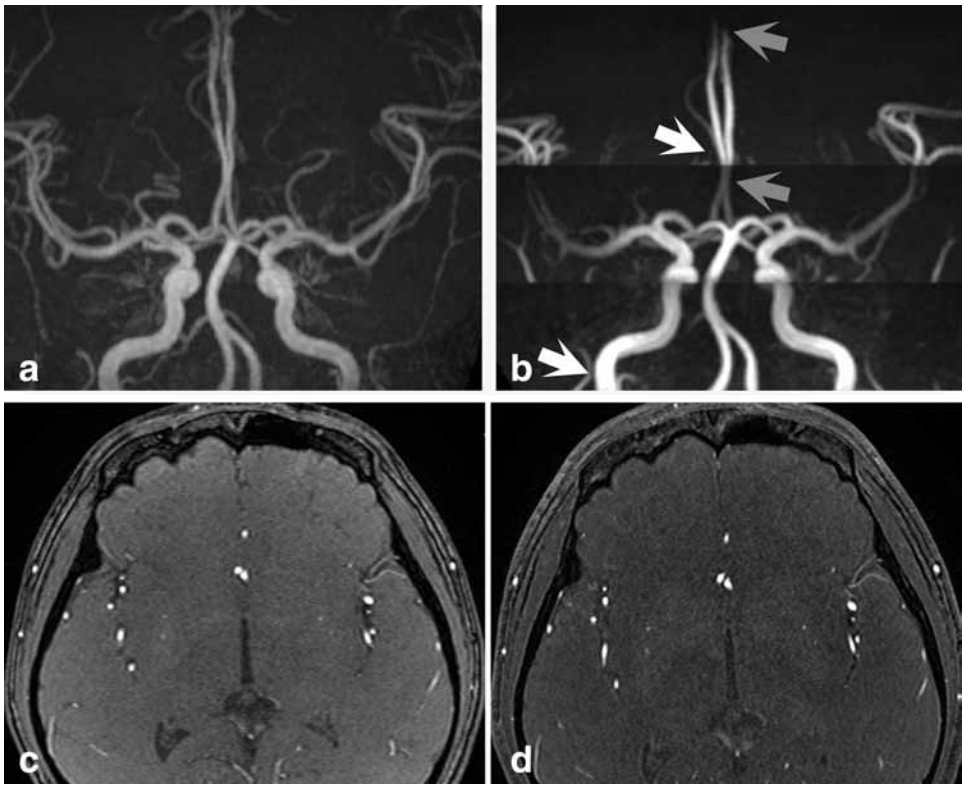

Figure 4. 3D TOF images in a normal volunteer demonstrate differences in vascular enhancement occurring when the flip angle is varied from (**a**) 15° to (**b**) 45°. In the latter image, vascular signal is greatest at areas of vascular in-flow into the slabs (white arrows), but diminished more distally within the slab (gray arrows) secondary to flow saturation effects. Images are shown with identical window and level settings. The source images from that volunteer obtained without (**c**) and with (**d**) a magnetization transfer preparatory pulse are also shown. As described in the text, the magnetization transfer preparation accentuates contrast between the vasculature and background tissues in MRA applications by suppressing signal from gray and white matter.

containing macromolecules relative to the blood pool which possesses fewer macromolecules, thus improving image contrast (16). One disadvantage of magnetization transfer pulses is the increased scan time. An example of the effect of magnetization transfer pulse use is provided in Fig. 4c,d.

PHASE-CONTRAST MRA

Introduction

Another widely used MRA technique is phase contrast. Phase contrast techniques allow quantitative flow analysis by mapping velocity-induced phase shifts of flowing blood. Phase-contrast MRA is commonly used in cardiac imaging, MR venography of the brain, and in other specialized scenarios requiring quantitative flow assessment (17,18). Figures 5 and 6 demonstrate this technique. Phase contrast techniques are usually performed using gradient echo acquisitions (19) but can also be done using alternative rapid imaging methods such as echo planar imaging (20). A typical phase-contrast velocity acquisition generates two series of cine images, a phase (Fig. 7a–c) and magnitude image (Fig. 7d). The magnitude image appears similar to a standard "bright-blood" gradient echo image and is used for anatomic localization. The phase image is a grayscale image where moving protons are depicted as either black or white, depending on the direction of their movement, and stationary tissues are represented as gray. The phase shift of a flowing proton is determined by its velocity and by the strength of the applied gradient and time of exposure to the gradient field. The phase images can therefore be used for flow and velocity measurements. Phase-contrast images, like TOF, can be obtained with 2D or 3D techniques. 2D techniques are typically cardiac-gated to allow for imaging of the vessels throughout the cardiac cycle. 3D acquisitions result in reduced voxel sizes but greater saturation effects and a significant acquisition time penalty. Decreasing the flip angle reduces problematic saturation effects, as does injecting gadolinium chelate contrast material. The latter can be used to allow utilization of a shorter TR, reducing acquisition time and improvement in small vessel visualization. Due to the longer acquisition times, 3D techniques are less frequently used clinically and are not typically cardiac-gated.

Flow-Encoding Gradients

Phase-contrast MRA depicts not only the presence of flow but also its direction. Flowing blood protons gain a specific phase relative to stationary protons when moving to different magnetic fields. The converse is

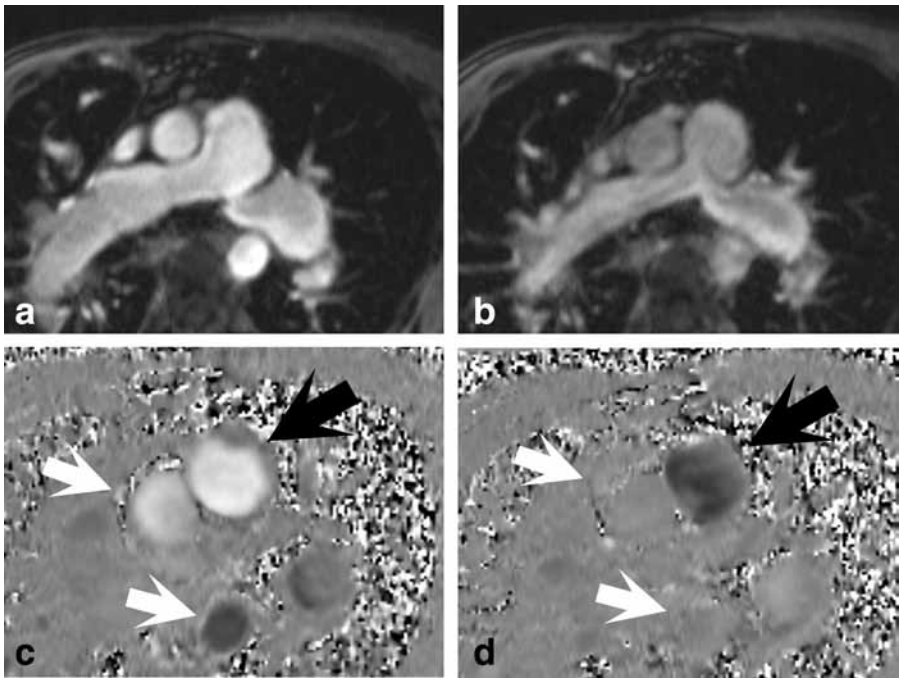

Figure 5. In this patient with pulmonary regurgitation, respective steady-state free precession (b-SSFP, ie, bright blood) in (**a**) systole and (**b**) diastole. Phase contrast images (**C,** systole; **D,** diastole) obtained at a slightly inferior slice position are also shown. Phase-contrast imaging confirmed the presence of pulmonary regurgitation: in these images, superiorly directed flow is depicted with high bright signal, inferiorly directed flow with dark signal, and lack of flow by intermediate signal (ie, gray in appearance). High bright signal is seen in the ascending aorta and dark signal in the descending aorta during in systole (C, white arrows). During diastole intermediate signal is seen in both the ascending and descending aorta (D, white arrows). Flow within the pulmonary artery during systole (C, black arrow) is also depicted as high bright signal. However, the pulmonary artery demonstrates a low signal intensity appearance in diastole, confirming the presence of pulmonary regurgitation (D, black arrow).

also true with blood protons losing phase upon moving to weaker magnetic fields. In both cases, the phase is directly proportional to the flow velocity. Phase-contrast techniques exploit this principle by application of an additional gradient (ie, a flow-encoding gradient). In a resulting image, objects without significant motion (or with motion perpendicular to the axis of the flow-encoding gradient) do not encounter any phase shift and are thus neither dark nor bright for reasons discussed below. The direction of flow-encoding is selectable. The effect of this selection is illustrated in Fig. 6.

In reality, flow is not the only factor contributing to phase shifts. Inhomogeneities in the local magnetic field also play a role, both with stationary and mobile protons. To compensate for this, two interleaved sequences are typically acquired: one sequence with velocity-compensation and a second velocity-encoded image with an additional encoding gradient added. A complex pixel by pixel subtraction of these images attempts to eliminate effects of field inhomogeneity on the final clinical image.

In addition to the axis on which the flow-encoding gradient is applied, signal intensity in phase-contrast imaging also depends on the duration and amplitude of such gradients. The velocity-encoding factor (VENC) reflects these parameters. If the VENC is set lower than the peak velocity present within the pixel being measured, signal from that pixel will artifactually appear opposite that of the adjacent pixels being measured due to a 360 wraparound of velocity information. To prevent this phase aliasing, the VENC must be greater than the highest flow velocity present. Alternatively, selecting too high a VENC can lead to loss of intravascular contrast compared with surrounding soft tissues. This is illustrated in Fig. 7. This principle is analogous to the selection of Doppler gain in sonography. The VENC can be specified for arterial (>100 cm/s) and venous assessments (~20–30 cm/s). An optimal VENC should be set within ~25% of the true peak velocity within the area being measured (21).

CONTRAST-ENHANCED MRA: BASIC PRINCIPLES

Introduction

Due to the ability to rapidly acquire images and the relative reduction in artifacts compared to the aforementioned TOF techniques, contrast-enhanced MRA has become the dominant clinically used MRA technique. In comparison to CTA, contrast-enhanced MRA evaluation is not impaired by the presence of atherosclerotic calcifications and does not subject the patient to ionizing radiation. Gadolinium chelate contrast media are the primary intravascular agents used in clinical contrast-enhanced MRA. Unlike CTA, where the presence of iodine accounts for changes in attenuation responsible for vessel enhancement, in

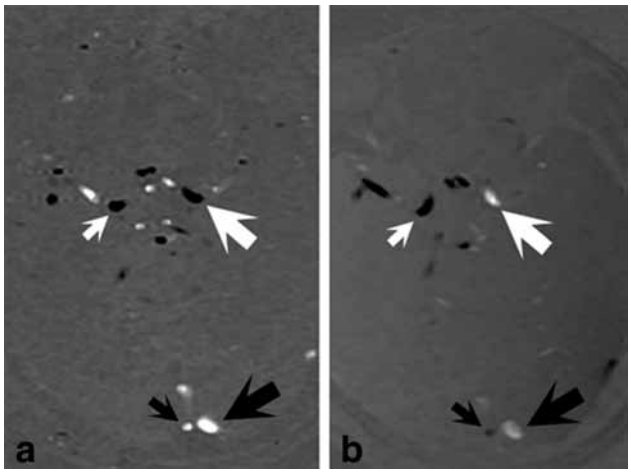

Figure 6. Axial phase-contrast images through the brain in a normal volunteer are displayed with the flow-encoding gradient directed (**a**) superior to inferior and (**b**) right to left. The direction of the flow-encoding gradient is typically selectable. With the gradient applied from superior to inferior, venous flow in both transverse sinuses (black arrows) is high signal intensity, denoting flow inferiorly, while arterial flow within the bilateral internal carotid arteries (white arrows) is low signal, denoting flow superiorly (the anterior cerebral arteries have a similar appearance). When the gradient is changed to span from the patient's right to left (b), the right carotid terminus (small white arrow), right middle cerebral artery, and right transverse sinus (small black arrow) demonstrate low signal intensity, denoting flow opposed to the direction of the gradient, whereas the left carotid terminus (large white arrow) and left transverse sinus (large black arrow) demonstrate high signal intensity, denoting flow in the direction of the flow-encoding gradient.

MRA the effects of gadolinium chelates are indirect. Gadolinium increases the rate of T1 recovery and T2 decay of the magnetization of protons in free water, and these effects are responsible for changes in blood signal relative to background. While T2* may be exploited in the setting of MR perfusion studies, for the purposes of routine MRA the extent of T1 relaxation is the most relevant parameter, allowing depiction of the vasculature as high signal intensity. A spoiled gradient echo technique is most frequently used, utilizing a short TE to minimize artifacts from susceptibility as well as flow-related signal loss. A short TR allows rapid image acquisition during the arterial phase of contrast enhancement. In some applications, particularly in peripheral vasculature imaging, subtraction images are constructed. This process consists of obtaining a precontrast scan used for subtraction from the final contrast-enhanced image, the subtraction of the two providing further contrast between intravascular signal and background tissue. Motion between these two sequences can markedly degrade image quality, although motion correction methods have been described to mitigate such problems (22).

Bolus Arrival and K-space

As with CTA, bolus timing is an important consideration with contrast-enhanced MRA. The major concern

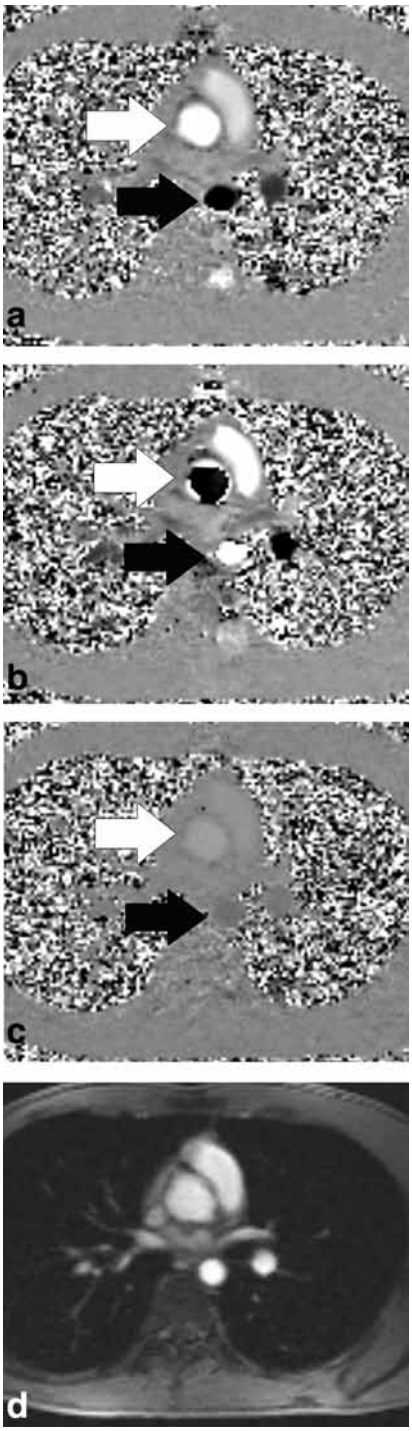

Figure 7. (**a–c**) Phase contrast and (**d**) magnitude images through the chest. The phase contrast images were performed with a VENC of (a) 150 cm/s, (b) 50 cm/s, and (c) 500 cm/s. With a VENC of 150 cm/s, cephalad directed flow is visualized by high, bright signal as in the ascending aorta (white arrow) and caudad flow with dark signal as in the descending aorta (black arrow). When the VENC is (b) chosen to be too low, there is marked aliasing or "wrap-around" within the ascending aorta (white arrow) manifest by central dark signal in the center of the vessel where flow has the greatest speed. The same effect results in high, bright signal throughout the descending aorta (black arrow). When the selected VENC is (c) too high, there is a loss of signal in structures with flow both cephalad and caudad.

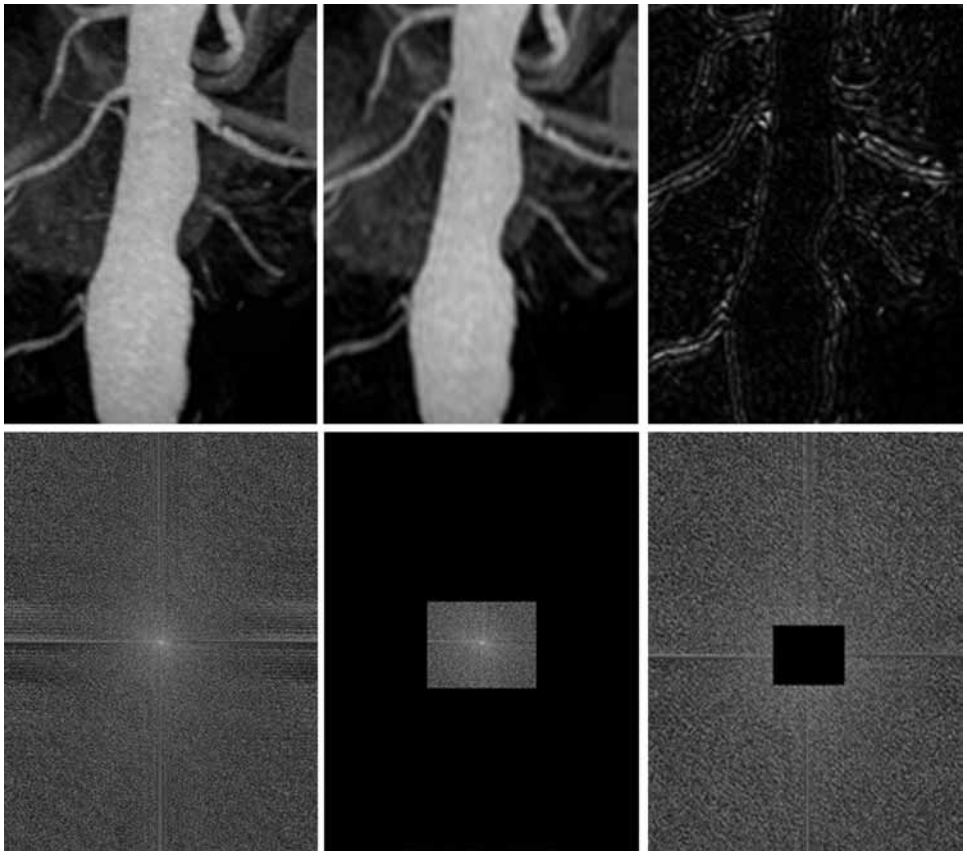

Figure 8. MIP images (top row) from a contrast-enhanced MRA examination in a patient with an infrarenal aortic aneurysm (partially visualized) and left renal artery stenosis. Inverse 2D Fourier transforms of the original image (bottom row) were performed using Corel Paintshop Pro X with an image processing plug-in (2D FFT/iFFT, Kamlex). Relevant portions of *k*-space data were then excluded as shown with a 2D Fourier transform subsequently performed. The center graphic depicts the effects of eliminating information encoded by the *k*-space periphery—namely, image blur with overall preservation of contrast between the vasculature and background. An additional image (right) depicts the effect of eliminating data from the *k*-space center, resulting in preservation of image detail information with a marked reduction in image contrast.

is synchronizing the acquisition of the central portion of *k*-space with the arrival of the contrast bolus. The *k*-space center encodes data relating to image contrast as opposed to the periphery, which encodes image detail. This is illustrated in Fig. 8. If the center of *k*-space is acquired prior to maximum arterial enhancement, arterial signal will be suboptimal and ringing artifacts may occur due to rapid increases in intravascular gadolinium chelate concentration (23). On the other hand, if image acquisition is delayed, then venous contamination may impair image quality.

K-space filling can proceed in a number of ways; however, elliptical centric ordering is often selected, whereby the *k*-space center is first acquired followed by peripheral data acquisition (24). Optimal coordination between the passage of the arterial bolus and acquisition of the central portion of *k*-space may likewise be achieved by a number of means. So-called bolus timing is one such technique by which a test bolus (typically 1–2 mL) is injected prior to the actual examination and its arrival in the target region is detected—typically with a series of fast 2D acquisitions. If the actual bolus is injected at a similar rate, then this provides an estimate of circulation time. For MRA images acquired at several different stations, an equal number of distinct test boluses may be used. In practice, this is rarely performed, as bolus chase techniques are often used where scan delays of later stations is determined by the acquisition time of earlier stations.

With bolus chasing techniques, the full imaging bolus is given with rapid scout images being acquired in temporal succession until bolus arrives within the region of interest. Whenever this occurs, as determined by the technologist manually or by computerized region of interest analysis, acquisition of the full scan begins with the most proximal anatomy being acquired first along with the contrast bolus. Each successive field of view (FOV) then follows the contrast bolus (ie, for the lower extremities down the abdomen, pelvis, and legs). Because of concerns regarding venous contamination in the lower extremities, many practices acquire an initial low-dose time-resolved MRA of the calves before performing the stepping table acquisition. Due to the different FOVs acquired, the obtained images must either be reviewed separately, with small areas of overlap, or be composed into a single image covering the entire region of clinical interest. Construction of composed images might

lead to potential artifacts at the demarcations between the different acquired FOVs.

The adoption of dedicated multielement coil systems and rapid scan acquisition with parallel imaging allow for continuous table movement MRA. In this case, the technologist only needs to plan a single large FOV. With this technique there is clearly no need for image composition, ensuring no overlap or exclusion of important vascular structures. Additionally, the lack of temporal gaps in imaging (ie, dead time while the table moves to a different station without image acquisition occurring) allows for more optimal coordination of image acquisition with arrival of the contrast bolus. This can allow more efficient bolus use. As alluded to above, requisites for this technique include implementation of parallel imaging, smooth and continuous table movement, multiple dedicated array coils for each body part that can be toggled on and off depending on the relation of that body part to the center of the magnet, and software, allowing integration of these factors and capable of producing images with minimal user input (25). A comparison of step-by-step and continuous table movement techniques is provided in Fig. 9.

Figure 9. Coronal oriented MIP images from a contrast-enhanced MRA from the thorax to the lower legs in two separate patients were obtained with (**a**) step-by-step MRA with three stations and (**b**) continuous table movement MRA. Figure is courtesy of Harald Kramer, MD. The latter patient exhibits multifocal stenoses and areas of occlusions throughout the vasculature secondary to atherosclerosis. In the step-by-step technique, the contrast bolus is followed as it progresses down the aorta and iliac arteries into the lower extremities. Oftentimes, an initial time-resolved single station MRA of the calves is performed, using a separate reduced dose, as a hedge against venous contamination in the final station of a step-by-step acquisition. In our example, signal drop-off between stations is accentuated. This can be made less prominent by overlapping the FOVs slightly by overlapping the stations. Here, intra-arterial signal within the calves is maximized, depicting three-vessel runoff bilaterally, but more superiorly arterial enhancement is somewhat diminished. These problems are not as apparent on the (b) continuous table movement images. Neither are the artifactual transitions between composed images obtained at the different stations (white arrows).

Postprocessing

Contrast-enhanced MRA images are typically acquired with 3D techniques, ideally with an isotropic voxel size. This allows for multiplanar reconstructions in any arbitrary imaging plane, a principle illustrated in the subtracted images provided in Fig. 10. Although subtraction was used with these images, subtracted images are usually not necessary in breath-held acquisitions of the chest and abdomen and can frequently lead to misregistration artifact. MIP images create an angiographic appearance by displaying the maximum pixel value along a given axis. These images are routinely used for interpretation in clinical MRA in combination with source images. Examination of the source images is imperative as important vascular and nonvascular structures may be excluded by the MIP filtering and subsequent postprocessing. Surface and volume rendering techniques are not typically used for interpretation by the radiologist. However, the latter may be more useful than MIP images for diagnosis in some cases (26,27). In the case of surface rendering, the first pixel value exceeding a specific threshold encountered along each parallel ray for a given axis is deemed the surface and is displayed as such in this type of reconstruction. A simulated light source creates the impression of a 3D image. The gray scale can likewise be modified and color added based on gray scale characteristics. Volume rendering is more complex: rather than simply selecting the first or maximum voxel value along a given axis, the average signal value is selected. Thus, signal differences are preserved while simultaneously allowing a 3D type depiction of anatomical structures. Averaging multiple pixel values can further diminish noise. Examples of MIP and volume-rendered images are provided in Fig. 11.

CONTRAST-ENHANCED MRA: DOSE REDUCTION

Nephrogenic Systemic Fibrosis (NSF)

One motivation for dose reduction in contrast-enhanced MRA may be reduction of the potential risk

Figure 10. Coronal, axial, and sagittal reconstructed subtraction images from a contrast-enhanced renal MRA performed with gadopentetate dimeglumine on a 1.5 T system demonstrate a short segment of greater 50% narrowing at the right renal artery origin. Acquisition with an isometric voxel size (1.0 mm^3) allows triplanar reconstruction. Although subtraction was used in this technique, image subtraction is usually not necessary in breath-held acquisitions of the chest and abdomen and can frequently lead to misregistration artifact.

for the development of NSF in patients with renal insufficiency. The pathophysiology of this condition is believed to relate to in vivo dechelation of gadolinium from the chelate complex with subsequent deposition of gadolinium—a toxic ion—into body tissues (28). The gadolinium chelates can be classified as linear or macrocyclic based on their structure—the latter available agents demonstrating greater in vitro stability (ie, lesser propensity to dechelate).

Relaxivity

The major determinant of image contrast obtainable with an extracellular gadolinium chelate is its relaxivity. Specifically in the context of MRA, the r1 relaxivity—or ability to reduce T1 of tissue protons—is an important consideration. Of note, such agents also reduce T2, secondary to T2* or susceptibility effects in much higher concentrations than used for MRA. In some contrast-enhanced applications, reductions in tissue T2 can interfere with T1 effects. This type of interference is a consideration with gadobenate dimeglumine at 3 T, where its r2 relaxivity increases disproportionately to that of other agents. However, for contrast-enhanced MRA, the TE values used are usually short enough so as to eliminate differences in enhancement related to r2 considerations. The major nonprotein binding extracellular gadolinium chelates demonstrate relatively similar r1 relaxivities, provided in Table 1, which are based on data from references (29,30). All agents are available

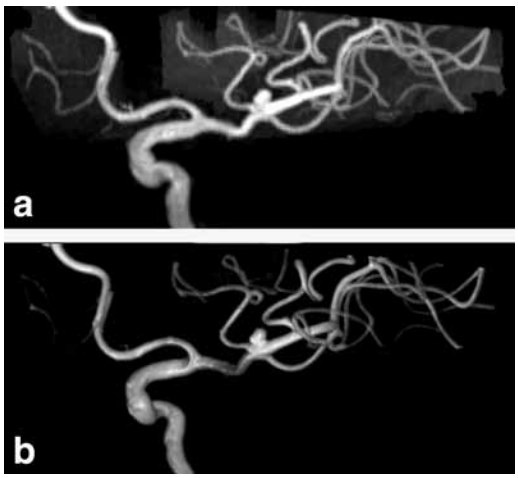

Figure 11. (**a**) MIP and (**b**) volume rendered images were constructed from a 3D TOF MRA examination of the Circle of Willis on a dedicated offline workstation (Siemens Leonardo). Images demonstrate a small saccular aneurysm at the trifurcation of the middle cerebral artery.

Table 1
Properties of Commonly Utilized Gadolinium Chelates

	R1 relaxivities[a]		Dissociation constant[b]	Molecular structure
Agent	1.5 T	3 T		
Gadoversetamide (Optimark)	4.7	4.5	15.0	Linear, nonionic
Gadodiamide (Omniscan)	4.3	4.0	14.9	Linear, nonionic
Gadobenate dimeglumine (Multihance)	6.3	5.5	18.4	Linear, ionic
Gadopentetate dimeglumine (Magnevist)	4.1	3.7	17.9	Linear, ionic
Gadobutrol (Gadavist)	5.2	5.0	15.5	Macrocyclic, nonionic
Gadoterate meglumine (Dotarem)	3.6	3.5	18.0	Macrocyclic, nonionic
Gadoteridol (Prohance)	4.1	3.7	17.7	Macrocyclic ionic

[a](L $mmol^{-1}$ s^{-1}) in plasma.
[b](Log K_{const}) at pH of 7.4 for linear agents and 1 for macrocyclic agents; higher coefficients correspond to greater stability for linear agents.
Shading indicates dissociation half-life of over 1000 years when extrapolated to pH 7.4.

commercially at concentrations of 0.5 molar with the exception of gadobutrol, which is available at 1 molar. Among the nonprotein binding agents, gadobutrol has the highest r1 relaxivity, the advantages of which are illustrated in Fig. 12a,b. Among the linear compounds, higher dissociation constants reflect greater stability (i.e. affinity of the chelate for gadolinium). Macrocyclic agents are overall more stable than the linear agents.

Protein-Binding Agents

Gadobenate dimeglumine, the single protein-binding agent listed in Table 1, demonstrates a greater relaxivity than its nonprotein-binding counterparts. The mechanism for this relates to the benzyloxymethyl group of the agent, which allows for transient interactions with albumin and other proteins. Because such proteins generally tumble at a slower rate than gadolinium chelates, such transient interactions likewise slow the tumbling of the chelate. With this reduction in tumbling, there is a more efficient interaction with water protons, improving relaxivity. The improved relaxivity of gadobenate dimeglumine allows the potential for significant dose reduction in many applications (31–33). Gadobenate dimeglumine, as well as gadofosveset trisodium, has been examined in the context of dose reduction. Gadofosveset sodium is a so-called "blood-pool" agent, with its intravascular persistence extending the window during which MRA and/or MR venography (MRV) can be obtained. Given the increased popularity of MRV for the detection of deep venous thrombosis, seen involving the left common iliac vein and inferior vena cava in Fig. 12c, gadofosveset sodium, with its prolonged intravascular persistence, creates a longer time period over which multistage or multiphase MR examinations can be performed. However, the issue of arterial segmentation has not been solved, particularly in the case of the lower extremity vessels, where paired veins lie immediately adjacent to very small calf arteries. In the chest and abdomen, extended acquisitions are also somewhat problematic on the basis of motion artifact. Respiratory-gated 3D MRA acquisitions are not widely available. An additional "protein-binding" agent worthy of mention is EP-2104R, although this agent is not yet available clinically. This peptide tetramer binds selectively to thrombin, allowing detection of vascular thrombi seen in thrombosis and, alternatively, fibrin within malignant neoplasms (34,35).

Parallel Imaging and 3 T

As illustrated by Table 1, the relaxivity of extracellular gadolinium chelates decreases at greater field strengths, in particular when moving from 1.5 to 3 T. However, the background tissue T1 time is increased at this higher field strength, leading to improved contrast between the enhancing vasculature and background for methods that do not employ image subtraction. Imaging at 3 T offers the most potential for clinical dose reduction based on this property. Furthermore, the advent of parallel imaging provides the means through which signal-to-noise ratio (SNR) gains seen with greater field strengths can be transformed into reductions in scan time or increases in spatial resolution (36). Parallel imaging refers to the ability of surface coils to localize MR signal, allowing for decreased sampling in the phase encoding directions, and thus a reduction in scan time. The use of parallel imaging is illustrated in Fig. 13.

SNR at a given location is inversely related to both the square root of the parallel imaging acceleration factor ($\sqrt{R}$) and the local geometry factor (g). The g factor reflects the ability of coil arrays to distinguish signal contributions and grows rapidly with increases in R (ie, geometry-related noise enhancement). Acceleration factors up to 3 are obtainable with 1D parallel imaging with geometry-related noise enhancement interfering at higher factors. This is manifest as regions of low SNR, often in the center of a large patient far from the location of the surface coil. In theory, parallel imaging can be applied in multiple directions simultaneously; however, few benefits in acquisition time would be seen by reducing sampling in the frequency encoding domain. Thus, parallel imaging is frequently limited to a single phase-encoding dimension, except for in 3D or multislice techniques, wherein parallel imaging can be applied along both phase encoding dimensions. Thus, the same scan time reduction effect of a parallel imaging factor of 4 can be achieved by utilizing factors of 2 in each direction (37). This enables a relatively lower geometry factor for the same total R. Of

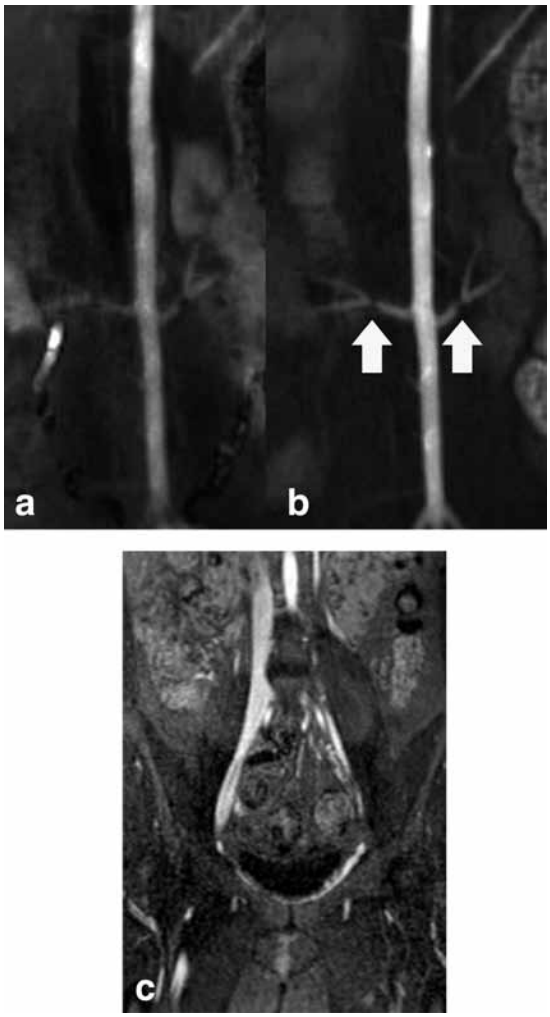

Figure 12. (**a**) Coronal MIPs from a time-resolved MRA of the renal arteries performed with equivalently dosed (0.02 mmol/kg) gadobutrol and (**b**) gadoterate meglumine on a single male swine with otherwise similar scan parameters. With identical windowing and leveling, the surgically created bilateral renal stenoses (white arrows) are better depicted on the gadobutrol scan. Aortic enhancement is also greater with gadobutrol. (**c**) A single coronal source image from MRV through the pelvis of a human patient utilizing gadobenate dimeglumine is also shown. Thrombus completely occludes the left common iliac vein with an additional filling defect noted in the inferior vena cava.

note, many coils are not compatible with this technique due to the orientation of their elements. In addition to loss of SNR, several artifacts are associated with parallel imaging. For example, in SENSE acquisitions if the calibration and parallel imaging acquisitions are not performed with the patient in the same position ghosting artifacts can result, or if the FOV of the calibration acquisition is smaller, signal voids can occur (38). Self-calibrating generalized autocalibrating partially parallel acquisition (GRAPPA) techniques can be used to avoid these problems; however, the acquisition of self-calibration lines of *k*-space is associated with an increased scan time, especially for low-resolution images where they occupy a greater proportion of the total acquisition.

DYNAMIC IMAGING

One of the major disadvantages of MRA relative to conventional angiography has traditionally been the relative lack of temporal resolution. Although the acquisition time could be reduced with MRA by also reducing spatial resolution, the advent of parallel imaging along with the development of 3 T MRA allowed the possibility of high-temporal (up to 1.5 sec per scan), high-spatial resolution MRA. Additional strategies such as TR reduction and partial Fourier sampling have aided in this goal. Different imaging techniques have been proposed that rely on preferential, repetitive sampling of the *k*-space center. As shown in Fig. 8, this region encodes image contrast information. Relative undersampling of *k*-space markedly improves temporal resolution versus conventional techniques in which the entirety of *k*-space is sampled. The sampling of the *k*-space periphery occurs near the end of the acquisition in "keyhole" techniques, but may be sampled dynamically as well. This typically occurs between acquisitions of the *k*-space center, either with different regions being sampled or with the entirety being sampled but with reduced sampling density. Several variations of this technique are available through different vendors, known by the acronyms TRICKS (Time-Resolved

Figure 13. MIP images from contrast-enhanced MRA examinations of the same patient at (**a**) 1.5 and (**b**) 3 T demonstrate occlusion of the left internal carotid artery. For images on the 1.5 T MR system, a parallel imaging factor of 2 was used with a voxel size of 0.9 × 1.3 × 1.0 mm, TE 1.3 msec, and TR 3.7 msec. For the 3 T scan, a parallel imaging factor of 3 was used with a voxel size of 0.8 × 0.8 × 0.8 mm, TE 1.14 msec, and TR 3 msec. Acquisition times were comparable. Twenty mL of gadoteridol was used in both cases. The greater resolution of the 3 T scan results in overall diminished image blur and allows improved depiction of small vascular structures such as the lingual and superior thyroid branches of the external carotid artery (white arrow).

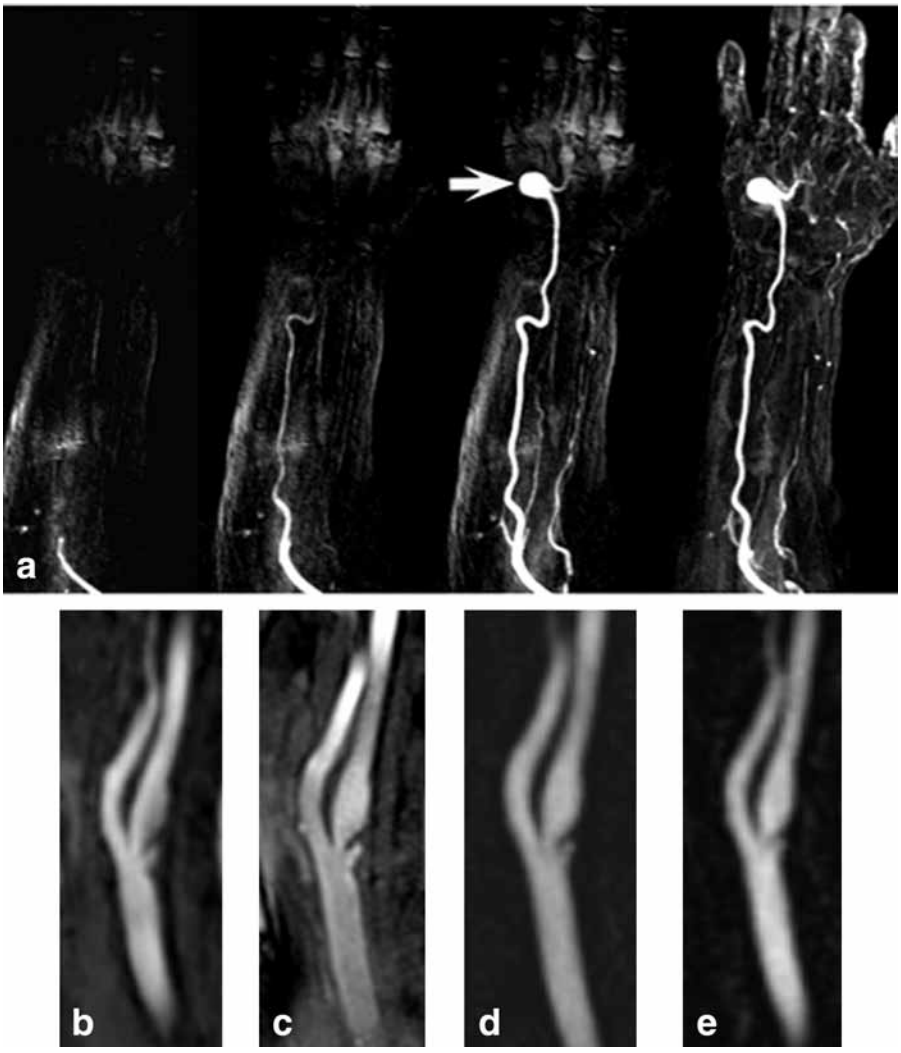

Figure 14. Sequential time-resolved, contrast-enhanced images through the upper extremity are shown (**a**) demonstrating a 1.6 cm pseudoaneurysm arising from the distalmost portion of the ulnar artery at its junction with the superficial palmar arch. The pseudoaneurysm neck measures 1 cm. On these MIP images, the portion of the arch overlying the 2nd metacarpal is not visualized, although this was patent on the source images. The radial artery and deep palmar arch are diseased, and not well seen. As illustrated here, directionality of flow is well-delineated with dynamic techniques. A shelf like stenosis is present in the proximal internal carotid artery as depicted on (**b**) TOF, (**c**) b-SSFP images with background suppression (Siemens NATIVE), (**d**) a standard postcontrast MRA examination, and (**e**) arterial phase images from a dynamic MRA dataset (Siemens TWIST). The provided images were all acquired at identical spatial resolutions (0.9 mm^3 isovoxel).

Imaging of Contrast KineticS) (39), TREAT (Time-Resolved Echo-shared Angiographic Technique) (40), and TWIST (Time-Resolved Angiography With Interleaved Stochastic Trajectories (41,42). With these view-sharing methods, an image is reconstructed from certain central data with other peripheral data points being used to complete *k*-space. Thus, the spatiotemporal resolution is nominally greater, but there is loss of temporal fidelity. The term "temporal footprint" refers to the time frame from which all data used for a single frame originate. Radial acquisitions can also be used to oversample the *k*-space center while undersampling the peripheral regions of *k*-space encoding high spatial frequencies; these techniques are typically less sensitive to motion artifacts (43).

Images from a time-resolved MRA sequences are illustrated in Fig. 14. Use of such dynamic techniques reduces problems from venous overlay. Further advantages with time-resolved techniques include a substantial contrast dose reduction with certain techniques, elimination of a test bolus, and reduction in motion artifact due to the shorter acquisition time for each frame. Additional temporal assessment of soft tissue enhancement available with this technique has been shown to be useful for detection of concomitant cellulitis in peripheral MRA applications (44).

Compressed sensing is another technique with a great deal of promise for accelerating dynamic MRA acquisitions. This is based on the fact that high lossy image compression ratios (ie, used for electronic image transfer) can be achieved without perceptible image quality degradation and while preserving diagnostic utility (45). Instead of collecting excess data only to have it discarded during compression, data are instead

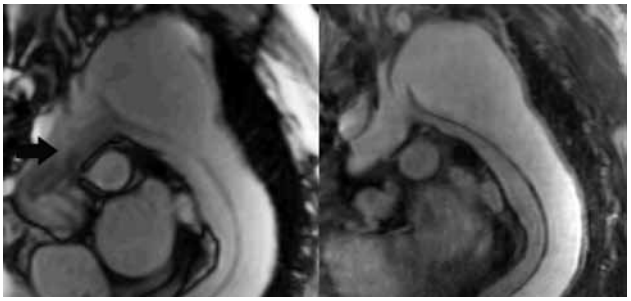

Figure 15. b-SSFP (left) and contrast-enhanced gradient echo sequences (right) were obtained as part of a thoracic MRA examination. An extensive Stanford type B dissection is shown. The true lumen is more anterior. Additionally, a 7.8 cm proximal descending aortic aneurysm is present. In this case, signal loss in the ascending aorta (black arrow) was felt to likely relate to turbulent flow within the ascending aorta due to the dissection.

undersampled. In the context of MRI, this is achieved by nearly randomly sampled *k*-space so that its undersampling leads to aliasing in no particular pattern (nonrandom sampling would lead to wraparound artifact). The resulting noise-pattern is not compressible and is suppressed with image compression. In initial experiments with CE-MRA, utilization of this technique has resulted in accelerations of image acquisitions up to 10-fold relative to conventional techniques with preservation of spatial resolution and contrast (46). Thus, acquisition of CE-MRA images with spatial resolutions comparable to those obtainable with conventional static MRA and also with high temporal resolution is expected to be possible clinically in the near future.

BALANCED STEADY-STATE FREE PRECESSION

Rather than spoiling residual transverse magnetization as in sequences used for TOF MRA, steady-state free precession sequences preserve this transverse magnetization across TR cycles, leading to superimposition of the spin echo upon the gradient echo component. However, phase shifts associated with rapidly flowing blood, as in MRA or cardiac imaging, degrade image quality. Application of balanced frequency, phase, and slice selection gradients can help to eliminate such phase shifts. Tissue contrast in b-SSFP sequences is dependent on T2/T1, a parameter maximized in the blood and cerebrospinal fluid (CSF). b-SSFP sequences are thus most well-known for their role in bright-blood cine imaging in cardiac imaging. Similarly, these techniques can be applied to noncontrast-enhanced MRA, achieving high accuracy (7,50). Compared to other noncontrast approaches such as TOF, flow-related exaggerations of vascular stenoses are less pronounced, as vascular signal with b-SSFP is relatively flow-independent. Artifacts due to turbulent flow can nevertheless occur, often in the context of valvular dysfunction in cardiac imaging, appearing as a low-signal intensity "jet" seen in the center of the vessel (47). TR is typically short and flip angles large, yielding high contrast-to-noise ratios and short acquisition times. Electrocardiogram (EKG)-gating may be useful, such as in the assessment of the thoracic aorta (48). An example of b-SSFP compared to traditional contrast-enhanced MRA is provided in Fig. 15. The principle disadvantage of b-SSFP with respect to image quality is artifacts secondary to off-resonance effects, principally owing to field inhomogeneity or susceptibility effects.

Modified 3D SSFP sequences have been adopted for use in noncontrast MRA of the abdomen and peripheral vasculature (49,50) as well as in carotid artery imaging (51). These techniques, which involve background suppression and inflow enhancement, are known by several vendor-specific acronyms (NATIVE by Siemens, InHance by GE, and TRANCE by Philips). For MRA, an initial IR RF pulse is applied to null stationary background and signal from slow-flowing venous blood. A b-SSFP sequence is then initiated during the recovery time, resulting in typical bright-blood signal associated with b-SSFP techniques. Because the IR RF pulse can be placed outside the imaging volume, this technique can also be used for MRV. An example of this technique is provided in Fig. 15 with comparison to other commonly used CE and non-CE MRA sequences. An alternative approach uses EKG gating to acquire TSE images during times of maximum and minimum blood flow (52). Subtraction of these datasets results in high intravascular signal. This technique relies on pulsatility and is better suited for use in areas with little patient motion (ie, lower extremities) due to reliance on image subtraction.

SUMMARY

With an increasing number and complexity of techniques in MRA, an image-based approach to understanding practical considerations is useful to radiologists. Through recognition of these underlying principles, the radiologist is more confident in changing sequence parameters to produce higher-quality imaging, personalizing the examination to the needs of the patient.

REFERENCES

1. Papke K, Brassel F. Modern cross-sectional imaging in the diagnosis and follow-up of intracranial aneurysms. Eur Radiol 2006;16:2051–2066.
2. Leiner T. Magnetic resonance angiography of abdominal and lower extremity vasculature. Top Magn Reson Imaging 2005;16:21–66.
3. Attenberger UI, Haneder S, Morelli JN, Diehl SJ, Schoenberg SO, Michaely HJ. Peripheral arterial occlusive disease: evaluation of a high spatial and temporal resolution 3-T MR protocol with a low total dose of gadolinium versus conventional angiography. Radiology 2010;257:879–887.
4. Scarabino T, Carriero A, Giannatempo GM, et al. Contrast-enhanced MR angiography (CE MRA) in the study of the carotid stenosis: comparison with digital subtraction angiography (DSA). J Neuroradiol 1999;26:87–91.
5. Morelli JN, Runge VM, Vu L, Loynachan AT, Attenberger UI. Evaluation of gadodiamide versus gadobutrol for contrast-enhanced MR imaging in a rat brain glioma model at 1.5 and 3 T. Invest Radiol 2010;45:810–818.
6. Attenberger UI, Runge VM, Morelli JN, Williams J, Jackson CB, Michaely HJ. Evaluation of gadobutrol, a macrocyclic, nonionic gadolinium chelate in a brain glioma model: comparison with gadoterate meglumine and gadopentetate dimeglumine at 1.5 T, combined with an assessment of field strength dependence, specifically 1.5 versus 3 T. J Magn Reson Imaging 2010;31:549–555.

7. Mohrs OK, Petersen SE, Schulze T, et al. High-resolution 3D unenhanced ECG-gated respiratory-navigated MR angiography of the renal arteries: comparison with contrast-enhanced MR angiography. AJR Am J Roentgenol 2010;195:1423–1428.
8. Willig DS, Turski PA, Frayne R, et al. Contrast-enhanced 3D MR DSA of the carotid artery bifurcation: preliminary study of comparison with unenhanced 2D and 3D time-of-flight MR angiography. Radiology 1998;208:447–451.
9. Leyendecker JR, Johnson SP, Diffin DC, Elsass K, Bifano SL. Time-of-flight MR arteriography of below-knee arteries with maximum-intensity-projection reconstruction: is interpretation of the axial source images helpful? AJR Am J Roentgenol 1997;169:1145–1149.
10. Wilcock DJ, Jaspan T, Worthington BS. Problems and pitfalls of 3-D TOF magnetic resonance angiography of the intracranial circulation. Clin Radiol 1995;50:526–532.
11. Barkhof F, Pouwels PJ, Wattjes MP. The Holy Grail in diagnostic neuroradiology: 3T or 3D? Eur Radiol 2011;21:449–456.
12. Haacke EM, Masaryk TJ, Wielopolski PA, et al. Optimizing blood vessel contrast in fast three-dimensional MRI. Magn Reson Med 1990;14:202–221.
13. Nagele T, Klose U, Grodd W, Petersen D, Tintera J. The effects of linearly increasing flip angles on 3D inflow MR angiography. Magn Reson Med 1994;31:561–566.
14. Ramgren B, Siemund R, Cronqvist M, et al. Follow-up of intracranial aneurysms treated with detachable coils: comparison of 3D inflow MRA at 3T and 1.5T and contrast-enhanced MRA at 3T with DSA. Neuroradiology 2008;50:947–954.
15. Henkelman RM, Stanisz GJ, Graham SJ. Magnetization transfer in MRI: a review. NMR Biomed 2001;14:57–64.
16. Atkinson D, Brant-Zawadzki M, Gillan G, Purdy D, Laub G. Improved MR angiography: magnetization transfer suppression with variable flip angle excitation and increased resolution. Radiology 1994;190:890–894.
17. Jeong HJ, Vakil P, Sheehan JJ, et al. Time-resolved magnetic resonance angiography: evaluation of intrapulmonary circulation parameters in pulmonary arterial hypertension. J Magn Reson Imaging 2011;33:225–231.
18. Shors SM, Cotts WG, Pavlovic-Surjancev B, Francois CJ, Gheorghiade M, Finn JP. Heart failure: evaluation of cardiopulmonary transit times with time-resolved MR angiography. Radiology 2003;229:743–748.
19. Spritzer CE, Pelc NJ, Lee JN, Evans AJ, Sostman HD, Riederer SJ. Rapid MR imaging of blood flow with a phase-sensitive, limited-flip-angle, gradient recalled pulse sequence: preliminary experience. Radiology 1990;176:255–262.
20. Mohiaddin RH, Gatehouse PD, Firmin DN. Exercise-related changes in aortic flow measured with spiral echo-planar MR velocity mapping. J Magn Reson Imaging 1995;5:159–163.
21. Chai P, Mohiaddin R. How we perform cardiovascular magnetic resonance flow assessment using phase-contrast velocity mapping. J Cardiovasc Magn Reson 2005;7:705–716.
22. Du J. Contrast-enhanced MR angiography with frequency-dependent mask subtraction. Magn Reson Imaging 2009;27:1326–1332.
23. Maki JH, Prince MR, Londy FJ, Chenevert TL. The effects of time varying intravascular signal intensity and k-space acquisition order on three-dimensional MR angiography image quality. J Magn Reson Imaging 1996;6:642–651.
24. Shetty AN, Bis KG, Vrachliotis TG, Kirsch M, Shirkhoda A, Ellwood R. Contrast-enhanced 3D MRA with centric ordering in κ-space: a preliminary clinical experience in imaging the abdominal aorta and renal and peripheral arterial vasculature. J Magn Reson Imaging 1998;8:603–615.
25. Kramer H, Zenge M, Schmitt P, Glaser C, Reiser MF, Herrmann KA. Peripheral magnetic resonance angiography (MRA) with continuous table movement at 3.0 T: initial experience compared with step-by-step MRA. Invest Radiol 2008;43:627–634.
26. Mallouhi A, Schocke M, Judmaier W, et al. 3D MR angiography of renal arteries: comparison of volume rendering and maximum intensity projection algorithms. Radiology 2002;223:509–516.
27. Mallouhi A, Felber S, Chemelli A, et al. Detection and characterization of intracranial aneurysms with MR angiography: comparison of volume-rendering and maximum-intensity-projection algorithms. AJR Am J Roentgenol 2003;180:55–64.
28. Morcos SK, Haylor J. Pathophysiology of nephrogenic systemic fibrosis: a review of experimental data. World J Radiol 2010;2:427–433.
29. Rohrer M, Bauer H, Mintorovitch J, Requardt M, Weinmann HJ. Comparison of magnetic properties of MRI contrast media solutions at different magnetic field strengths. Invest Radiol 2005;40:715–724.
30. Juluru K, Vogel-Claussen J, Macura KJ, Kamel IR, Steever A, Bluemke DA. MR imaging in patients at risk for developing nephrogenic systemic fibrosis: protocols, practices, and imaging techniques to maximize patient safety. Radiographics 2009;29:9–22.
31. Attenberger UI, Runge VM, Jackson CB, et al. Comparative evaluation of lesion enhancement using 1 M gadobutrol vs. 2 conventional gadolinium chelates, all at a dose of 0.1 mmol/kg, in a rat brain tumor model at 3 T. Invest Radiol 2009;44:251–256.
32. Nural MS, Gokce E, Danaci M, Bayrak IK, Diren HB. Focal liver lesions: whether a standard dose (0.05 mmol/kg) gadobenate dimeglumine can provide the same diagnostic data as the 0.1 mmol/kg dose. Eur J Radiol 2008;66:65–74.
33. Bauner KU, Reiser MF, Huber AM. Low dose gadobenate dimeglumine for imaging of chronic myocardial infarction in comparison with standard dose gadopentetate dimeglumine. Invest Radiol 2009;44:95–104.
34. Morelli JN, Runge VM, Williams JM, Beissner RS, Tweedle M. Evaluation of a fibrin-binding gadolinium chelate peptide tetramer in a brain glioma model. Invest Radiol 2011;46:169–177.
35. Vymazal J, Spuentrup E, Cardenas-Molina G, et al. Thrombus imaging with fibrin-specific gadolinium-based MR contrast agent EP-2104R: results of a phase II clinical study of feasibility. Invest Radiol 2009;44:697–704.
36. Londy FJ, Lowe S, Stein PD, et al. Comparison of 1.5 and 3.0 T for contrast-enhanced pulmonary magnetic resonance angiography. Clin Appl Thromb Hemost 2012;18:134–139.
37. Weiger M, Pruessmann KP, Boesiger P. 2D SENSE for faster 3D MRI. MAGMA 2002;14:10–19.
38. Glockner JF, Hu HH, Stanley DW, Angelos L, King K. Parallel MR imaging: a user's guide. Radiographics 2005;25:1279–1297.
39. Turski PA, Korosec FR, Carroll TJ, Willig DS, Grist TM, Mistretta CA. Contrast-Enhanced magnetic resonance angiography of the carotid bifurcation using the time-resolved imaging of contrast kinetics (TRICKS) technique. Top Magn Reson Imaging 2001;12:175–181.
40. Fink C, Ley S, Kroeker R, Requardt M, Kauczor HU, Bock M. Time-resolved contrast-enhanced three-dimensional magnetic resonance angiography of the chest: combination of parallel imaging with view sharing (TREAT). Invest Radiol 2005;40:40–48.
41. Morelli JN, Ai F, Runge VM, et al. Time-resolved MR angiography of renal artery stenosis in a swine model at 3 Tesla using gadobutrol with digital subtraction angiography correlation. J Magn Reson Imaging 2012;36:704–713.
42. Morelli JN, Runge VM, Ai F, et al. Magnetic resonance evaluation of renal artery stenosis in a swine model: performance of low-dose gadobutrol versus gadoterate meglumine in comparison with digital subtraction intra-arterial catheter angiography. Invest Radiol 2012;47:376–382.
43. Jeong HJ, Eddleman CS, Shah S, et al. Accelerating time-resolved MRA with multiecho acquisition. Magn Reson Med 2010;63:1520–1528.
44. Zhang HL, Kent KC, Bush HL, et al. Soft tissue enhancement on time-resolved peripheral magnetic resonance angiography. J Magn Reson Imaging 2004;19:590–597.
45. Vasanawala SS, Alley MT, Hargreaves BA, Barth RA, Pauly JM, Lustig M. Improved pediatric MR imaging with compressed sensing. Radiology 2010;256:607–616.
46. Lustig M, Donoho D, Pauly JM. Sparse MRI: the application of compressed sensing for rapid MR imaging. Magn Reson Med 2007;58:1182–1195.
47. Krombach GA, Kuhl H, Bucker A, et al. Cine MR imaging of heart valve dysfunction with segmented true fast imaging with steady state free precession. J Magn Reson Imaging 2004;19:59–67.
48. Krishnam MS, Tomasian A, Malik S, Desphande V, Laub G, Ruehm SG. Image quality and diagnostic accuracy of unenhanced SSFP MR angiography compared with conventional contrast-enhanced MR angiography for the assessment of thoracic aortic diseases. Eur Radiol 2010;20:1311–1320.

49. Glockner JF, Takahashi N, Kawashima A, et al. Non-contrast renal artery MRA using an inflow inversion recovery steady state free precession technique (Inhance): comparison with 3D contrast-enhanced MRA. J Magn Reson Imaging 2010;31: 1411–1418.
50. Serai S, Towbin AJ, Podberesky DJ. Non-contrast MRA using an inflow-enhanced, inversion recovery SSFP technique in pediatric abdominal imaging. Pediatr Radiol 2012;42:364–368.
51. Kramer H, Runge VM, Morelli JN, et al. Magnetic resonance angiography of the carotid arteries: comparison of unenhanced and contrast enhanced techniques. Eur Radiol 2011;21: 1667–1676.
52. Lanzman RS, Blondin D, Schmitt P, et al. Non-enhanced 3D MR angiography of the lower extremity using ECG-gated TSE imaging with non-selective refocusing pulses—initial experience. Rofo 2010;182:861–867.

Non-Contrast Enhanced MR Angiography: Physical Principles

Andrew J. Wheaton, Ph.D. and Mitsue Miyazaki, Ph.D.*

Reprinted with permission from the ISMRM Journal of Magnetic Resonance Imaging: Volume 36: Pages 286 - 304, (C) 2012 with permission from Wiley-Liss, Inc.

This article is accredited as a journal-based CME activity. If you wish to receive credit for this activity, please refer to the website: www.wileyhealthylearning.com

ACCREDITATION AND DESIGNATION STATEMENT

Blackwell Futura Media Services designates this journal-based CME activity for a maximum of 1 *AMA PRA Category 1 Credit*™. Physicians should only claim credit commensurate with the extent of their participation in the activity.

Blackwell Futura Media Services is accredited by the Accreditation Council for Continuing Medical Education to provide continuing medical education for physicians.

EDUCATIONAL OBJECTIVES

Upon completion of this educational activity, participants will be better able to discuss the primary applications, advantages, and limitations of established and emerging NCE-MRA techniques.

ACTIVITY DISCLOSURES

No commercial support has been accepted related to the development or publication of this activity.

Faculty Disclosures:

The following contributors have no conflicts of interest to disclose:

Editor-in-Chief: C. Leon Partain, MD, PhD

CME Editor: Scott B. Reeder, MD, PhD

CME Committee: Scott Nagle, MD, PhD, Pratik Mukherjee, MD, PhD, Shreyas Vasanawala, MD, PhD, Bonnie Joe, MD, PhD, Tim Leiner, MD, PhD, Sabine Weckbach, MD, Frank Korosec, PhD

Authors: Andrew J. Wheaton, PhD, Mitsue Miyazaki, PhD

This manuscript underwent peer review in line with the standards of editorial integrity and publication ethics maintained by *Journal of Magnetic Resonance Imaging*. The peer reviewers have no relevant financial relationships. The peer review process for *Journal of Magnetic Resonance Imaging* is double-blinded. As such, the identities of the reviewers are not disclosed in line with the standard accepted practices of medical journal peer review.

Conflicts of interest have been identified and resolved in accordance with Blackwell Futura Media Services's Policy on Activity Disclosure and Conflict of Interest. No relevant financial relationships exist for any individual in control of the content and therefore there were no conflicts to resolve.

INSTRUCTIONS ON RECEIVING CREDIT

For information on applicability and acceptance of CME credit for this activity, please consult your professional licensing board.

This activity is designed to be completed within an hour; physicians should claim only those credits that reflect the time actually spent in the activity. To successfully earn credit, participants must complete the activity during the valid credit period.

Follow these steps to earn credit:

- Log on to www.wileyhealthylearning.com
- Read the target audience, educational objectives, and activity disclosures.
- Read the article in print or online format.
- Reflect on the article.
- Access the CME Exam, and choose the best answer to each question.
- Complete the required evaluation component of the activity.

This activity will be available for CME credit for twelve months following its publication date. At that time, it will be reviewed and potentially updated and extended for an additional period.

Toshiba Medical Research Institute, Vernon Hills, Illinois, USA.
*Address reprint requests to: M.M., Toshiba Medical Research Institute, 706 N. Deerpath Dr., Vernon Hills, IL 60061.
E-mail: mmiyazaki@tmriusa.com
Received July 14, 2011; Accepted February 15, 2012.
DOI 10.1002/jmri.23641
View this article online at wileyonlinelibrary.com.

Noncontrast-enhanced magnetic resonance angiography (NCE-MRA) methods have been demonstrated in anatomies throughout the body. Previously established NCE-MRA techniques suffered from long scan times or low sensitivity. Advances in hardware and software have made NCE-MRA scan times clinically feasible. Recent concerns over the safety of gadolinium-based contrast material combined with the expense of the material and its administration have generated a demand for NCE-MRA. In response, several new NCE-MRA methods have been developed. The physical mechanisms underlying five general classes of NCE-MRA methods (inflow effect, flow-dependency on cardiac phase, flow-encoding, spin labeling, and relaxation) are explained. The original techniques of time-of-flight (TOF) and phase contrast MRA (PC-MRA) are briefly introduced. New developments in NCE-MRA, including hybrid of opposite-contrast (HOP-MRA), four dimensional PC-MRA (4D Flow), cardiac-gated 3D fast-spin-echo, flow-sensitive dephasing (FSD), arterial spin labeling (ASL), and balanced steady-state free-precession (bSSFP) are highlighted. The primary applications, advantages, and limitations of established and emerging NCE-MRA techniques are discussed.

Key Words: angiography; noncontrast; unenhanced; MRA
J. Magn. Reson. Imaging 2012;36:286–304.

MAGNETIC RESONANCE ANGIOGRAPHY (MRA) applications have been a general application of MRI practice since the inception of clinical MRI. The first applications of MRA were performed without exogenous contrast enhancement. These techniques leveraged the MR-related differences between flowing and stationary spins to generate depictions of bright vessels on a dark background. These techniques, including time-of-flight (TOF) and phase contrast (PC), were the earliest developments of noncontrast-enhanced MRA (NCE-MRA).

The use of gadolinium-based contrast enhancement for MRA (CE-MRA), introduced in 1994 (1), greatly accentuated the signal from inflowing blood via the T1-shortening effect of gadolinium, resulting in improved angiograms. The seminal work by Prince was demonstrated on abdominal MRA, but soon thereafter CE-MRA techniques were refined for use in practically all anatomical regions (1–4). Due to its excellent image quality and speed, and spurred by improvements in MR hardware, software, and receiver coils, CE-MRA was rapidly adopted by the radiology, cardiology, and vascular communities for widespread routine clinical practice.

Development of modern NCE-MRA techniques has been motivated by several factors. Historically, Japan has been a source of NCE-MRA development due to the restriction of a maximum administration of 20 cc of contrast material per patient by the Japanese Ministry of Health, Labor, and Welfare (5). Perhaps the greatest source of Japanese interest in NCE-MRA stems from the persistently high cost of contrast material relative to clinical MR scan reimbursement by the Japanese medical establishment. Although contrast material is not as relatively expensive in other parts of the world, the added cost of contrast material combined with time, personnel, and equipment for set-up and administration of the contrast injection are additional motivators for the clinical use of NCE-MRA over CE-MRA.

Beyond cost-savings, safety-related motivations for avoiding contrast enhancement have compelled global development of NCE-MRA. Concerns about a possible link between gadolinium-based contrast agents and nephrogenic systemic fibrosis (NSF) have brought into question the use of these agents for MRA (6,7). While this link has not yet been conclusively proven, a correlative association has been identified by several studies (8–12). As a precaution, the U.S. Food and Drug Administration applied a black-box warning on gadolinium-based contrast agents in 2007 (13). Due to NSF concerns, it is recommended that special considerations be taken regarding the use of gadolinium-based contrast agents, especially for renal-compromised patients (7,14,15). The confounding factor is that it is often the renal-compromised patients who are the patient population that needs an MRA examination.

The recent renaissance in NCE-MRA owes as much to technical advancements in MR hardware and software as it does to its cost- and safety-related motivating factors. Multichannel receiver coil arrays generate higher signal-to-noise ratio (SNR), which can be exchanged for higher resolution. High bandwidth data acquisition hardware combined with faster and stronger gradients facilitate shorter TEs and TRs, enabling faster scan times, higher SNR, and/or higher-resolution images. The application of parallel imaging techniques in NCE-MRA has reduced shot durations and/or the total number of shots, thereby greatly reducing scan times (16,17). The higher field strength of the increasingly prevalent 3T scanners not only improves SNR, but also lengthens T1, resulting in reduced stationary tissue signal in inflow-based NCE-MRA and longer blood transit times for spin labeling NCE-MRA. Although these advancements have enabled the progress of MRI in general, since NCE-MRA methods have had traditionally longer scan times, lower resolution, and lower SNRs compared to CE-MRA, the combination of these technical improvements has been particularly important in making NCE-MRA applications feasible for routine clinical use.

This review article examines both established and recently developed NCE-MRA techniques. These techniques are categorized by their dominant mechanism: inflow, flow-dependency on cardiac phase, flow-encoding, spin labeling, and relaxation. The purpose of this review article is to explain the physical mechanism underlying each method and discuss their relative advantages and disadvantages. In particular, the characteristics of each technique are highlighted with regard to coverage efficiency, scan time, sensitivity to vessel orientation, vessel selectivity, venous contamination, and background suppression. For each technique a brief overview of the clinical applications is provided. A more detailed description of the clinical applications using these techniques can be found in complementary review articles (18–20). Other relevant principles of MRA, such as arterial and venous flow patterns and T1 and T2 values of arteries and veins, are discussed elsewhere (18–23).

Focusing on angiography, other general blood-flow-related techniques will not be explored including perfusion applications of spin labeling, quantification of cardiac function, or vessel imaging using black-blood methods. While noncontrast-enhanced venography can be accomplished with some of the techniques (24), the primary focus will be on arteriography.

INFLOW-BASED TECHNIQUES

General Mechanism of Inflow Effect

The oldest class of NCE-MRA techniques relies on the inflow effect of blood, also known as time-of-flight (TOF) (25,26). The inflow effect is the result of the difference in exposure to radiofrequency (RF) excitation of spins in stationary tissue versus spins in inflowing blood. Repeated RF excitation of a section (slice or slab) saturates stationary spins causing their longitudinal magnetization (M_z) to approach a low steady-state value ($M_z \approx 0$), resulting in low image signal intensity. However, inflowing blood entering the section arrives with fresh longitudinal magnetization ($M_z = 1$), resulting in high image signal intensity.

The inflow effect is dependent on the refilling rate of the section. The percentage of the blood that is refreshed within a section is a function of blood velocity, repetition time (TR), and cross-sectional area of the vessel (related to the section thickness). Figure 1 illustrates the inflow effect. For a simple plug-flow model, if blood velocity > thickness/TR, the entire volume of blood within the section is replaced between RF excitations. If the blood velocity is less than this critical replacement velocity, some portion of the blood volume will experience multiple RF excitations and become partially saturated. In this partial saturation regime the blood signal is dependent on the excitation flip angle and the T1 of blood. It is this flip angle/T1 dependency that CE-MRA exploits due to the fast gadolinium-assisted T1 relaxation of contrast-enhanced blood (1).

Inflow-based techniques are commonly paired with a flow-compensated readout to reduce signal loss from flow-induced spin dephasing (25,26). These flow-compensated gradient waveforms use extra gradient lobes to null gradient moments for both stationary spins and flowing spins moving through the gradient field. Flow-compensated gradient waveforms can be applied on either or all of the readout (RO), phase encode (PE), or slice select (SS) axes. Sequences like balanced steady-state free-precession gradient-echo (bSSFP, trueFISP, FIESTA, trueSSFP, bFFE) can also be used for MRA due to the inherent flow-compensation provided by the moment balancing of bSSFP.

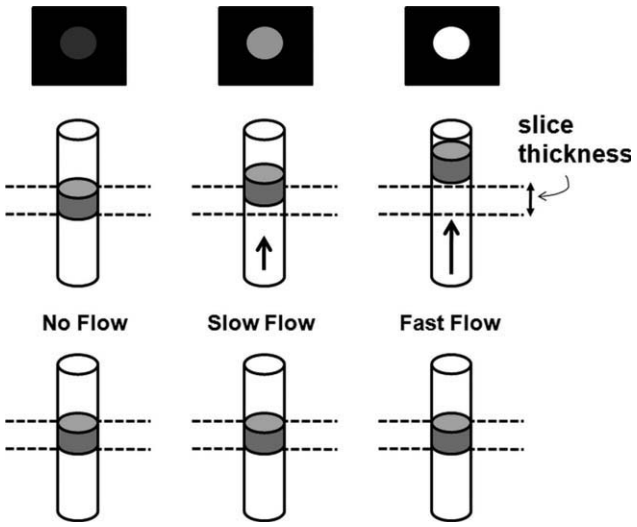

Figure 1. Illustration of the inflow effect. Bottom row: Spins within the imaging section (dotted lines) are excited by the excitation RF pulse. Middle row: After one TR period, stationary spins remain within the imaging section. Slow-flowing spins have partially flowed out of the imaging section and are partially replaced by fresh inflowing spins. Fast-flowing spins have flowed out of the imaging section and are completely refreshed by inflowing spins. Top row: pictorial images of the inflow effect. Stationary spins are repeatedly saturated and produce near zero signal. Slow-flowing spins are partially saturated and produce low signal. Fast-flowing spins are unsaturated at each excitation and produce high signal.

General Limitations of Inflow-Based Techniques

In inflow-based techniques, any inflowing blood, whether from venous or arterial sources, arrives with fresh longitudinal magnetization ($M_z = 1$) and appears bright. Hence, the inflow-based techniques are prone to venous contamination. To generate an arteriogram with minimal venous contamination, venous suppression is often incorporated using a "walking" presaturation RF pulse. This selective presaturation RF pulse is applied to the venous upstream region relative to the imaging section. As the imaging section is spatially shifted to the next position, the venous presaturation region position is shifted proportionately to "walk" with the imaging section. In this way the relative distance between the venous presaturation region and the imaging section, and hence the venous suppression effect, is held constant.

The inflow effect is dependent on the vessel orientation relative to the imaging section. The optimal refreshment occurs for arteries running perpendicular to the thinnest dimension of the section volume. For vessels that lie generally in parallel with the imaging section their effective refreshment rate is very low. For this reason, inflow-based techniques are most applicable for vessels with preferential orientations like the carotid or peripheral arteries. For more tortuous vessels like renal arteries or distal peripheral arteries in the hand or foot, the refreshment rate is drastically reduced and hence inflow-based techniques are rarely used in these anatomies.

3D TOF

Description

The thick slab of 3D acquisitions poses a challenge for inflow-based techniques. The blood velocity needs to be very high to refresh the thick slab, so most often 3D TOF operates in the partial saturation regime. To address this issue the slab can be split into multiple,

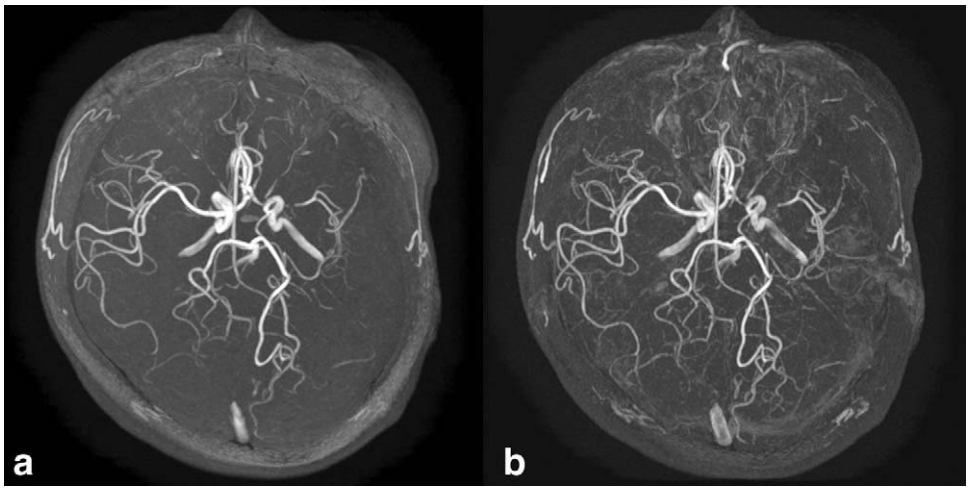

Figure 2. Comparison of axial projection MIP for (**a**) 3D TOF and (**b**) HOP-MRA at 3T on a 14-year-old girl with moyamoya disease. The HOP-MRA image shows increased conspicuity of small vessels compared to the conventional 3D TOF image. (Image courtesy of Dr. K. Tsuchiya, Kyorin University Hospital, Tokyo, Japan.)

thinner slabs. By using thinner slabs the critical replacement velocity is reduced, resulting in increased inflow refreshment. Often, the multiple slab coverages are partially overlapped, reducing coverage efficiency. Further enhancements to the thin slab approach include multiple overlapping thin-slab acquisition (MOTSA) (27,28). This hybrid 2D/3D method is designed to greatly reduce the effective selection thickness and increase the inflow effect. To further reduce blood saturation, the slab can be excited using an RF excitation pulse with ramped slice selection profile like the tilted optimized nonsaturating excitation (TONE) pulse (29). The TONE pulse reduces saturation for spins entering the slab by using a low flip angle at the inflow edge and a higher flip angle at the outflow edge. To further suppress stationary tissue signal, a nonselective off-resonance magnetization transfer (MT) RF pulse can be applied to reduce the signal of brain parenchyma (29–31). Brain parenchyma is more susceptible to MT saturation than blood due to its greater relative macromolecular content.

Applications

The most common application of 3D TOF is intracranial angiography (25–36). In particular, 3D TOF has been used for diagnostic imaging of intracranial occlusions (32,33) as well as aneurysms (34,35). The high resolution of the 3D acquisition provides excellent depiction of small intracranial vessels. Since physiological motion is negligible in the head, long scan times (>5 minutes) to acquire high-resolution images are acceptable (36).

HOP-MRA

Description

The hybrid of opposite-contrast (HOP) MRA method is an extension of 3D TOF (37). The HOP-MRA pulse sequence begins with a flow-compensated echo acquisition, similar to conventional 3D TOF. The first echo is typically flow-compensated in all three axes. Within the same TR, following the first flow-compensated echo, a second flow-spoiled echo is acquired. Between the first and second echoes, flow-dephasing bipolar gradients (see Flow-Encoding section for further description) are applied to all three axes to dephase flowing spins, which results in a dark appearance of blood. The echo data are reconstructed into two separate images: bright-blood and dark-blood. Since it is fundamentally 3D TOF, the bright-blood image depicts fast-flowing blood better than slow-flowing blood. On the other hand, the dark-blood image generates negative contrast even for slow-flowing spins, including those in small branch arteries. The bright-blood and dark-blood images are combined using subtraction to yield a final angiogram (38). The combined angiogram benefits from the strengths of each source image; it is able to depict vessels with both fast- and slow-flowing blood in a single angiogram created from a single scan. Furthermore, stationary tissue signal is mostly eliminated via subtraction, thereby enhancing vessel depiction.

Applications

The intended application of HOP-MRA is the same as 3D TOF: intracranial angiography (37–39). Figure 2 illustrates the additional fine vessel structure depicted by HOP-MRA compared to conventional 3D TOF.

2D TOF

Description

The thinner sections of 2D TOF allow faster inflow refreshment and increased arterial signal compared to 3D TOF-based methods. However, since the 2D slice thickness is typically larger (≥3 mm) than the slice resolution of 3D TOF (≤1 mm), the 2D TOF approach is commonly used only for angiography of large gauge vessels. Often, the 2D slices are acquired with some overlap to reduce the discontinuities at the slice edges in a maximum intensity projection (MIP) depiction of the data—often called the "stairstep artifact" (40,41). This 2D overlap reduces the coverage efficiency of the technique. The 2D TOF technique is notorious for depicting false stenoses at the carotid notch due to reduced inflow refreshment caused by the angle of the vessel orientation (42). Also, the 2D TOF technique commonly generates signal voids in the carotid bulb due to recirculating flow patterns (43).

Figure 3. Coronal MIP of a multi-station peripheral run-off study on a volunteer using QISS. Axial QISS data were acquired with 1 × 1 mm in-plane resolution and 3 mm effective slice thickness (interpolated to 1.5 mm). In this example, the total scan time for all stations was approximately 6 minutes 30 seconds. (Image courtesy of Dr. R. Edelman, NorthShore University Health System, Evanston, IL.)

Applications

The 2D TOF technique is commonly used for imaging vessels with preferentially perpendicular flow and relatively fast velocity like peripheral (41) and carotid (43) arteries. It has been demonstrated for the evaluation of stenosis in tibial and pedal arteries (41). In peripheral applications, 2D TOF is often combined with systolic gating to capture the period of greatest blood velocity, and hence greatest inflow effect.

QISS

Description

Recently, an inflow-based NCE-MRA technique called quiescent interval single-shot (QISS) has been developed (44). The QISS technique relies on a presaturation RF pulse to saturate the signal in the imaging slice. Following the presaturation, during a "quiescent interval" (QI) fresh inflowing blood enters the saturated slice. The signal is quickly acquired using a single-shot 2D bSSFP sequence. The trigger delay is adjusted so systole occurs during the QI and signal acquisition occurs during diastole. By aligning the QI with systole, maximum inflow is achieved. The 2D slice is moved sequentially from foot to head so the slice can be continually filled with fresh, unsaturated, inflowing blood. The QI is designed to be long enough to allow adequate inflow, but short enough to maintain saturation of the stationary tissue signal. Since the QI is relatively long compared to the short T1 of fat, a fat saturation prepulse is commonly applied immediately prior to bSSFP readout.

QISS differs from 2D TOF with regard to sensitivity and speed. The inflow refreshment effect is much greater for QISS than 2D TOF. The QI period (≈230 msec) allows for a relatively long time for inflow refreshment compared to a typical TR of 2D TOF (≈30 msec). This greatly reduces the critical replacement velocity, thus making QISS able to depict slow-flowing blood. For a 3-mm slice, full inflow refreshment can be achieved for QISS by blood flowing at 1.3 cm/s versus 10 cm/s for the equivalent 2D TOF slice.

Applications

The use of QISS is dictated by some of the same limitations as 2D TOF. The slice orientation of QISS should be perpendicular to the general vessel orientation to improve the inflow effect. Therefore, its most common application is for run-off studies in peripheral arteries (Fig. 3) (44). Due to its use of the bSSFP readout, QISS requires good B_0 homogeneity across the image volume. Therefore, the useable extent of field-of-view (FOV) and slice coverage is limited by the quality of the static magnetic field (B_0) shim. Accordingly, QISS is often performed with a greater number of smaller coverages with reshimming between each coverage acquisition. Since QISS acquires a complete slice in one cardiac R-R period (≈1 sec), QISS is able to cover a 15-cm region using a 3-mm slice thickness in 1 minute versus 5 minutes for 2D TOF with similar parameters. A multi-station run-off study (iliac to calf station) using QISS takes ≈8–10 minutes, not including time for repositioning or reshimming.

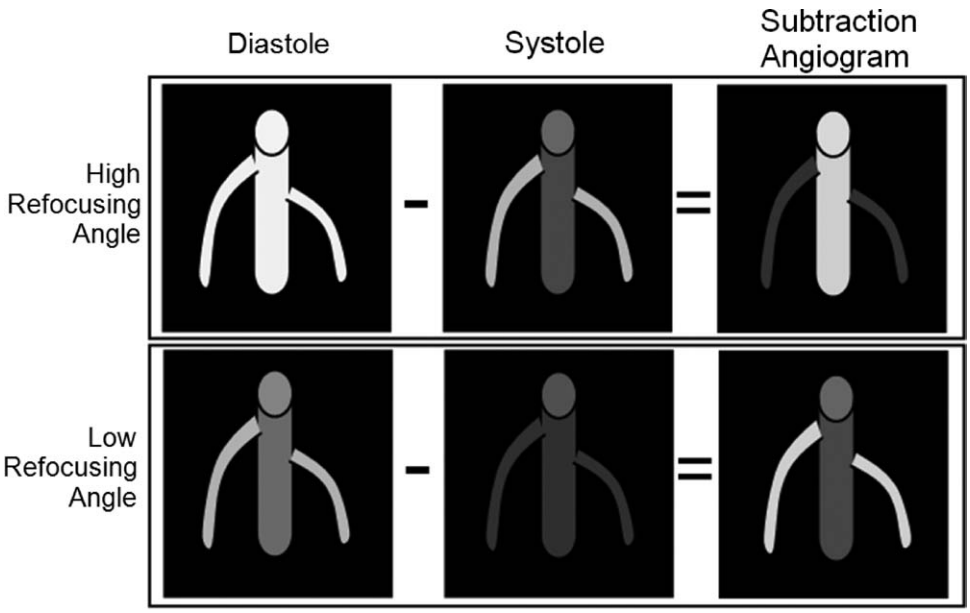

Figure 4. Illustration of the effect of refocusing flip angle on vessel signal in diastole (bright-artery scan) and systole (dark-artery scan). The large central artery contains fast-flowing blood and the two smaller branch arteries contain slow-flowing blood. With high refocusing angles, although the small vessels are relatively bright in both systole and diastole scans, due to subtraction, they appear dark in the angiogram. Due to low refocusing angles, the large artery signal is reduced in both diastole and systole scans, resulting in weak depiction in the subtraction angiogram.

CARDIAC PHASE-DEPENDENT TECHNIQUES

General Mechanism of Flow-Dependency on Cardiac Phase

The cardiac-phase-dependent class of NCE-MRA techniques relies on the physiologic difference in arterial flow velocity between systolic and diastolic cardiac phases. During systole, arterial flow is fast, whereas during diastole arterial flow is slower. In contrast, venous flow is nonpulsatile and relatively slow (<5 cm/s) throughout the cardiac cycle.

This general class of NCE-MRA techniques leverages the motion sensitivity of pulse sequences to produce dark-artery (DA) image sets acquired during systole and bright-artery (BA) image sets acquired during diastole. The DA image set is subtracted from the BA image set to create the angiogram. Ideally, the signal from stationary tissue in both image sets is identical and therefore cancels in the final subtracted image. The motion-sensitization of the technique can be generated or accentuated in several ways, which is further described below.

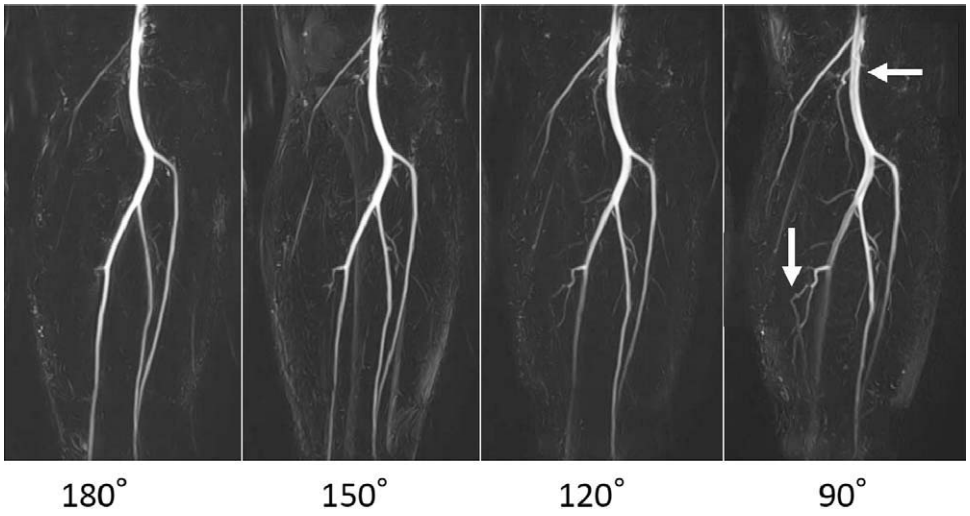

Figure 5. Example of the cardiac-gated 3D FSE NCE-MRA method in the popliteal region. Each image is a coronal MIP of the coronally acquired 3D FSE image volume. The corresponding refocusing angle used in the FSE acquisition is listed below each MIP. The horizontal arrow near the femoral artery highlights the signal loss in large arteries due to the low refocusing angle. The vertical arrow near the posterior tibial artery highlights the improved depiction of branch vessels with low refocusing angle.

Cardiac-Gated 3D Fast-Spin-Echo NCE-MRA

Description

The fast-spin-echo (FSE, or turbo-spin-echo TSE) sequence, including half-Fourier FSE or single-shot FSE, is inherently sensitive to motion. Spins flowing out of the imaging section during the echo train cannot be repeatedly refocused by the RF refocusing pulses. This signal void is the premise behind thin-slice black-blood 2D FSE (45). However, in NCE-MRA, thick-slab 3D FSE is used, so this source of flow-related signal loss is minor and little flow-spoiling is observed in the slice direction. The strongest flow-spoiling effect for 3D FSE is in the RO direction due to the alternate echo flow-spoiling effect caused by the RO gradients in the echo train. In both the slice and RO directions, the flow-spoiling effect is exacerbated by the use of sub-180° refocusing flip angles in the echo train, resulting in even greater signal loss. Essential concepts related to angiography applications of FSE, including flow-compensation (46), gradient moment nulling (47), and the T2-blurring effect (48,49) are discussed elsewhere.

The inherent flow-spoiling of FSE is the underpinning of cardiac-gated 3D FSE NCE-MRA. The original 2D projection spin-echo-based technique (50,51) was later refined and extended to a 3D NCE-MRA technique (52,53). Cardiac-gated 3D FSE NCE-MRA produces images with dark signal (flow void) in arteries with fast-flowing blood to create the systolic DA scan. The slower blood flow during diastole generates high arterial signal in the BA scan. Since the venous flow is relatively constant in both image sets, venous contamination is effectively removed via subtraction in the final angiogram. This method is available commercially as FBI, NATIVE SPACE, 3D Delta Flow, and TRANCE.

The fast-spin-echo readout commonly uses only one or two shots per slice encoding value to minimize total scan time. Each shot uses a partial-Fourier echo train to shorten the echo train length to reduce T2-blurring. The RO direction is typically selected to be in parallel with the general direction of flow to accentuate the flow-spoiling effects of FSE (54). The scan is triggered with either electrocardiographic (ECG) or peripheral pulse gating (PPG). The ideal systolic and diastolic trigger delay times are calibrated per patient. Often, the image sets are acquired with fat suppression, typically using short-tau inversion recovery (STIR) or spectrally adiabatic inversion recovery (SPAIR). While fat suppression is not strictly necessary due to the subtraction step which removes stationary tissue signal, the removal of fat improves the image quality in the native DA and BA source image sets since they are often diagnostically evaluated alongside the subtracted angiogram (54). The DA and BA image sets are acquired in direct succession to mitigate patient motion and reduce image misregistration. Thus, the total scan time for both systolic and diastolic acquisitions using cardiac-gated 3D FSE NCE-MRA is in the range of 3–4 minutes (54). A typical multi-station run-off study (iliac to calf station) takes ≈10–12 minutes, not including time for repositioning or recalibration of cardiac delay times (54).

The motion sensitivity of cardiac-gated 3D FSE NCE-MRA techniques is influenced by the choice of refocusing flip angle (55). The refocusing flip angle affects the relative depiction of fast-flowing blood in large arteries versus slow-flowing blood in smaller branch arteries, as illustrated in Figure 4 and exemplified in Figure 5. High refocusing flip angles (160°+) produce very bright signal in BA scans, but also refocus more signal in arteries with slow-flowing blood in DA scans. Thus, a high refocusing flip angle produces a subtraction angiogram with bright signal for large arteries, but weak signal for small arteries. Low refocusing flip angles (<120°) produce lower signal for large arteries in BA scans, but small arteries with slower diastolic flow are less affected. The low refocusing angle accentuates the FSE flow-spoiling effect, resulting in reduced arterial signal in the DA scan, even in smaller arteries with slow-flowing blood. Thus, a low refocusing flip angle produces a subtraction angiogram with greater signal intensity in smaller arteries and less signal intensity in larger arteries. Accordingly, the proper refocusing flip angle can be tuned depending on the arteries of interest.

In a similar fashion, the flow sensitivity of cardiac-gated 3D FSE NCE-MRA can also be adjusted by adding additional flow-dephasing or partially flow-compensating gradient lobes in the RF echo train (53,54). If additional flow-dephasing is added, the scan is able to better depict slow-flowing blood. In the same manner as the lower refocusing flip angle, using readout gradients with additional flow-dephasing generates a subtraction angiogram with relatively higher signal in smaller arteries and weaker signal in larger arteries. To better depict fast-flowing blood in large arteries, such as the iliac, partially flow-compensating readout gradients are commonly applied for the opposite effect. The partial flow-compensation makes the readout gradients become less susceptible to signal loss caused by flow-induced dephasing. Thus, similar to the use of a high refocusing angle, the BA scan and the DA scan both produce high signal for slow-flowing blood in small arteries. The result is a subtraction angiogram with bright signal in large arteries and weaker signal in smaller arteries.

Unlike the inflow-based techniques, the choices of FOV and section thickness have no impact on the angiographic applications of the technique, other than simple SNR and coverage efficiency considerations. Since the cardiac-gated 3D FSE NCE-MRA readout method is insensitive to B_0 inhomogeneity, cardiac-gated 3D FSE NCE-MRA can be used with robust results near susceptibility fields (lungs) or with large FOV coverage.

The cardiac-gated 3D FSE NCE-MRA techniques have some fundamental limitations. Since these techniques are cardiac-gated, they are sensitive to the effects of arrhythmia or trigger delay calibration errors. Due to the requirement of two scan acquisitions and multiple R-wave intervals, the methods are generally slow. Due to the inherent flow-spoiling effects of FSE, very fast and/or turbulent flow, like poststenotic flow, generates a flow void even in the BA scan (42). Since the BA scan and the DA scan depict

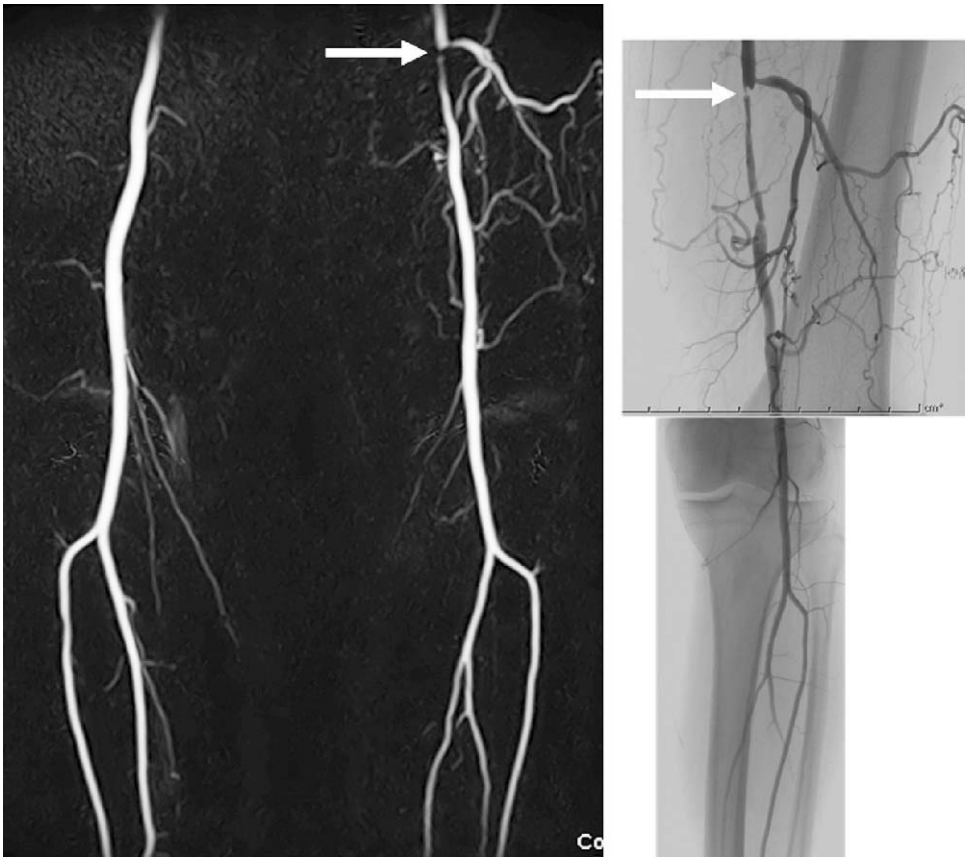

Figure 6. Example of cardiac-gated 3D FSE NCE-MRA (left) compared to x-ray digital subtraction angiography (right) on a patient with peripheral occlusive disease. The occlusion is indicated by an arrow on each image. (Image courtesy of Dr. J. Levine, Little Company of Mary Hospital, Evergreen Park, IL.)

vessels with low signals in this region, a signal void appears in the subtraction angiogram leading to a tendency toward overestimation of stenosis. This overestimation can be mitigated by evaluation of BA images in conjunction with the subtraction angiogram (54).

Applications

The large coronal FOV coverage, robustness to B_0 inhomogeneity, inherent venous suppression, and insensitivity to vessel orientation enable the widespread application of cardiac-gated 3D FSE NCE-MRA. Since the FSE readout can capture vessel signal close to air–tissue interfaces, a common application is pulmonary angiography. Cardiac-gated 3D FSE NCE-MRA has been used in angiography of the thoracic and abdominal aorta (5). Near the thoracic and abdominal aorta, the acquisition can be performed with a single diastolic BA scan to produce an angiogram with minimal background signal since venous and stationary tissues are largely absent in this region.

The cardiac-gated 3D FSE NCE-MRA method is well suited for peripheral run-off MRA due to its large volume coverage. Several clinical studies comparing cardiac-gated 3D FSE NCE-MRA to computed tomography angiography (CTA) (54) and CE-MRA (56,57) in peripheral run-offs reported high diagnostic scores of sensitivity (97%, 85.4%, and 100%, respectively) and negative predictive value (NPV) (99%, 92.3%, and 100%, respectively). However, the clinical studies reported lower diagnostic scores for specificity (96%, 75.8%, and 72.7%–85.5%, respectively) and positive predictive value (PPV) (88%, 74.1%, and 66.7%–78.2%, respectively). In addition, the CE-MRA comparison studies (56,57) reported that 47.2% and 42.4%, respectively, of segments in cardiac-gated 3D FSE NCE-MRA data were deemed nondiagnostic due to image artifacts.

A modified cardiac-gated 3D FSE NCE-MRA technique using variable flip angles has also been applied in angiography of the hands at 3T incorporating additional flow-dephasing gradients to enhance the depiction of slow-flowing blood in the arteries of the extremities (58). Figure 6 shows an example of cardiac-gated 3D FSE NCE-MRA and x-ray digital subtraction angiography (DSA) on a patient with peripheral occlusive disease.

FLOW-ENCODING TECHNIQUES

General Mechanism of Flow-Encoding

In the same way that magnetic field gradients can be used to encode the spatial position of spins, they can be used to encode the motion, or flow, of spins. Spins in the transverse plane flowing in the vector direction of a gradient field accumulate phase proportional to their speed. In this way, the flow velocity (direction and speed) is encoded in the phase of the spins. Bipolar gradients consisting of two equal but opposite amplitude gradient lobes are commonly used for flow-encoding. The bipolar gradients generate net zero phase for stationary spins but a nonzero phase for flowing spins related to the amplitude and duration of

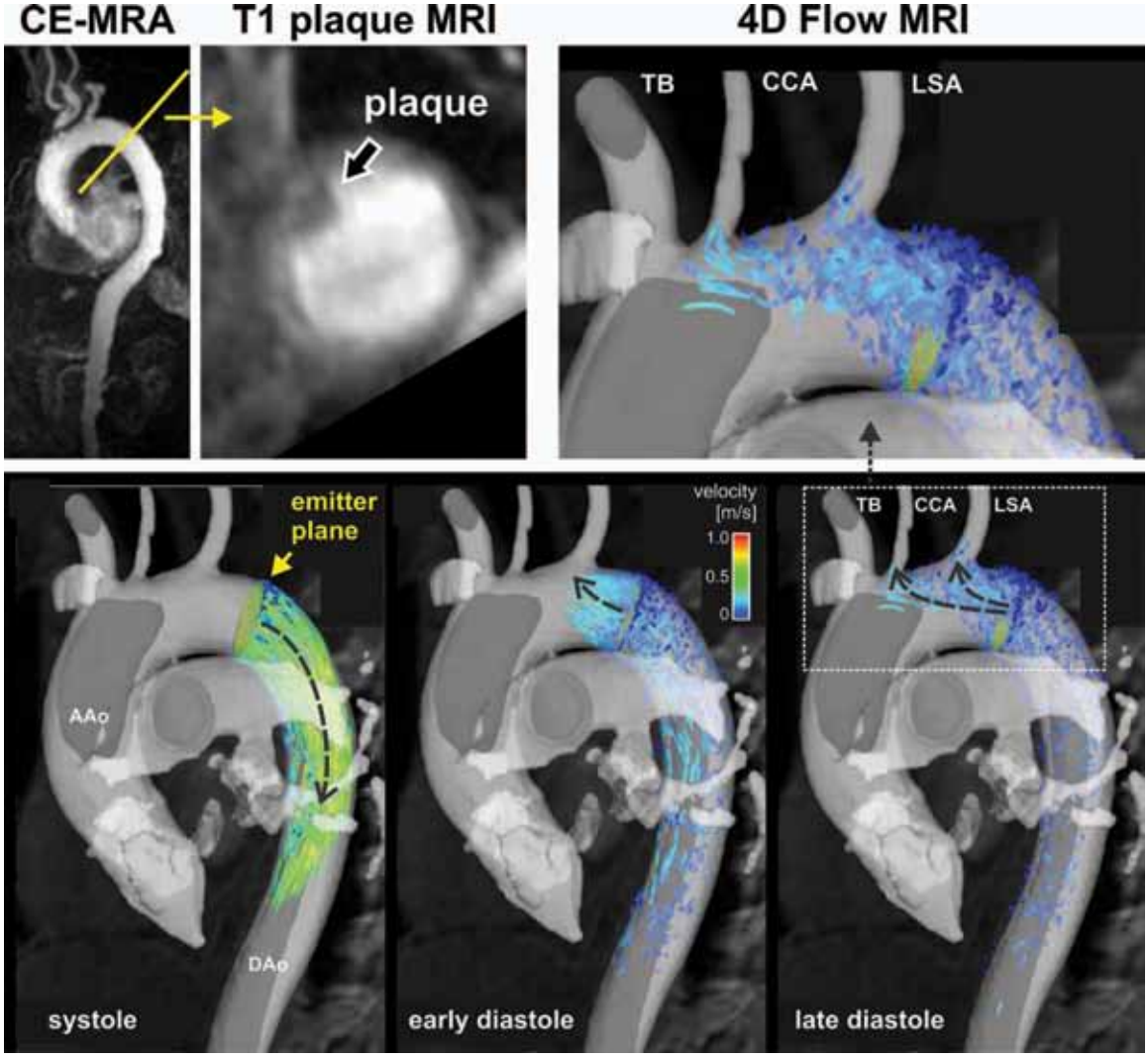

Figure 7. Top row: CE-MRA and 3D T1 plaque MRI used for detecting the location and size of aortic high-risk plaques. The plaque image shows a hypointense structure protruding into the proximal descending aorta (DAo) with a superimposed mobile thrombus ≥8 mm. CE-MRA indicates plaque localization. Lower row: An emitter plane positioned at the location of the aortic plaque was used to generate time-resolved 3D particle traces, which resemble the temporal and spatial evolution of blood flow throughout the cardiac cycle. The series of images show systolic forward flow followed by substantial diastolic retrograde flow. Marked diastolic retrograde flow originating from the location of the plaque in the proximal descending aorta is clearly evident and reaches two of three brain-feeding arteries. This mechanism thus indicates a risk for retrograde embolization in the brain stem and left hemisphere in the case of plaque rupture. (Image courtesy of Dr. M. Markl, Northwestern University, Chicago, IL.)

the bipolar gradient lobes. Alternatively, the flow-induced phase can be used for simple flow-dephasing instead of flow-encoding.

Conventional Phase Contrast

Description

Phase contrast MRA (PC-MRA) uses flow-encoding bipolar gradients to generate quantitative flow images (59–61). Since the flow information is encoded in phase, for PC-MRA, phase rather than magnitude images are reconstructed. For the simplest case of 1D flow quantification, two PC scans are acquired. Typically, alternate bipolar polarities are used (+/− followed by −/+). By subtracting the two flow-encoded PC phase images, the background phase accrual is removed. Since stationary spins have zero net phase after the subtraction, stationary tissue signals are inherently suppressed in the displayed phase difference images. Quantitative measurements of flow velocity can be calculated from the phase data using the explicit relationship between velocity and bipolar gradient amplitude and duration. These quantitative data are presented as a flow map.

Since the bipolar gradients can be applied in any combination of RO, PE, or SS axes, PC-MRA can be used to measure directionality of flow as well as speed. Thus, PC-MRA has the advantage of depicting multidirectional flow, including recirculating flow patterns. Unlike inflow-based techniques, which require blood to flow through the slice to be visible, PC-MRA

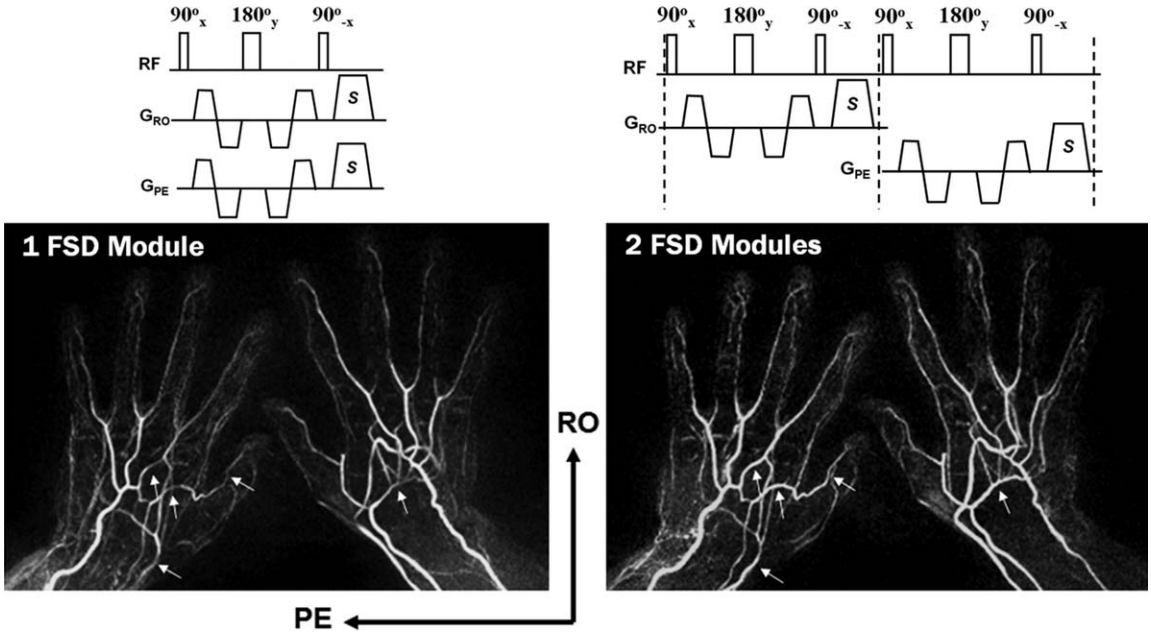

Figure 8. Example of FSD in the digital arteries. By using two FSD modules in succession with orthogonal flow-dephasing gradient directions (RO axis followed by PE axis), the arterial depiction is improved compared to using only one FSD module with a single flow-dephasing gradient direction (simultaneously applied on RO and PE axes). The arrows on the images indicate vessels with signal improvement using the two-module versus the one-module approach. (Image courtesy of Dr. Z. Fan, Northwestern University, Chicago, IL.)

can detect flowing blood that remains within the slice. In its simplest form, PC-MRA requires two images to generate flow data in a single direction. To visualize flow in orthogonal directions, additional directional pairs must be acquired at the cost of adding proportionally more scan time.

Applications

Due primarily to its long scan times, PC-MRA is not commonly used for routine MRA beyond specific niche applications. Its most common angiographic use is as a low-resolution scout sequence for identifying the location of the carotid arteries. PC-MRA has also been used to distinguish the degree of stenosis in renal (62) and carotid (63) arteries.

4D Flow

Description

An emerging application of PC-MRA is the measurement of flow dynamics with 4D flow mapping (64). The fourth dimension in this application is time. The technique generates time-resolved 3D PC flow maps acquired with cine mode ECG gating. The fundamental techniques behind 4D flow have existed for some time, but only recently have hardware and software advances enabled the time resolution of the acquisition as well as the processing and visualization capabilities to generate high-quality results.

Applications

Visualization of hemodynamics using the 4D flow technique affords a comprehensive evaluation of regional aortic flow characteristics. The 4D flow technique has been applied to the measurement of aortic pulse wave velocity (65) and wall shear stress (66) for the purposes of identifying potential emboli from high-risk atherosclerotic plaque (67). Figure 7 shows an example of 4D flow analysis of atherosclerotic plaque in the aorta.

Flow-Sensitive Dephasing

Description

Recently, an alternative flow-encoding-based technique called flow-sensitive dephasing (FSD) has been developed (68). The FSD module consists of a 90°(x)-180°(y)-90°(−x) spin-echo interspersed with optional flow-encoding bipolar gradients (Fig. 8). In the FSD technique, the flow-induced phase generated by the bipolar gradients is not used for flow-encoding, but rather flow-dephasing. At the RF echo, the flipback 90°(−x) RF pulse restores rephased transverse magnetization in stationary tissue to the longitudinal axis. The dephased spins in flowing blood remain in the transverse plane to be further crushed by the trailing gradient. The motion sensitivity of FSD can be controlled by the amplitude and duration of the bipolar gradient lobes. This sensitivity is commonly referred to in the literature as "m1" in reference to the first-order moment the flow-dephasing gradients impart on flowing spins. High m1 corresponds to strong flow-dephasing effect, whereas m1 = 0 corresponds to no flow-dephasing.

The FSD technique also relies on the general mechanism of flow-dependency on cardiac phase. The DA scan is acquired with high m1 during systole using ECG or PPG gating. Specifically, the trigger delay is calibrated to align the timing of the FSD prepulse

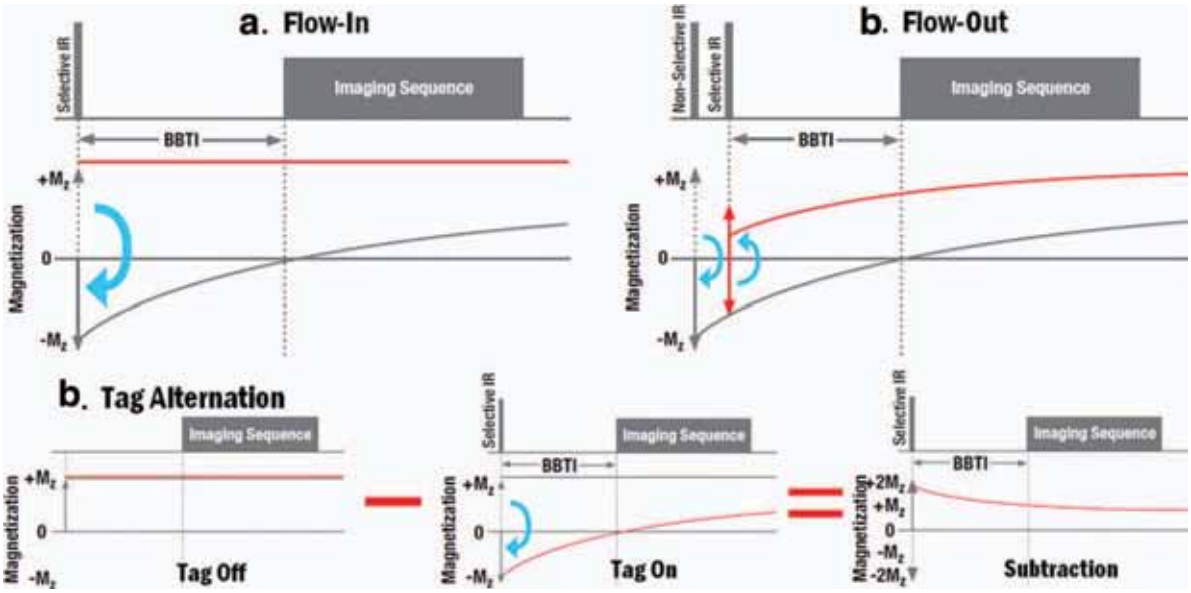

Figure 9. Illustration of the different spin labeling methods: (**a**) flow-in, (**b**) flow-out, and (**c**) tag-alternation. Refer to Figure 10 for an illustration of the tag placement relative to the image volume for each method. A: Flow-in: following a selective inversion pulse (typically corresponding to spatial region of the imaging volume) blood (red line) with fresh magnetization flows into the imaging volume during the BBTI period while the stationary tissue (gray line) undergoes T1 recovery. Data acquisition occurs near the null point of stationary tissue. B: Flow-out: An initial nonselective inversion pulse inverts all magnetization. Immediately afterward, a selective inversion pulse, applied to a separate vessel tagging region, restores magnetization only within the tagging region. During the BBTI, the restored blood flows into the imaging volume while stationary tissue undergoes T1 recovery. C: Tag-alternation: the tag-off acquisition acquires an image with blood and stationary tissue with positive magnetization. The tag-on acquisition uses a selective inversion pulse (applied to a separate vessel tagging region) to invert magnetization only within the tagging region. During the BBTI, the inverted blood flows into the imaging volume. The subtraction of tag-on from tag-off data produces an angiogram with positive signal in regions fed by inflowing blood and null signal in stationary tissue.

with the arrival of the systole bolus. The high m1 of the flow-dephasing gradients generates low arterial signal in the DA scan. The BA scan is acquired with m1 = 0 during diastole, resulting in high arterial signal. The DA magnitude image set is subtracted from the BA magnitude image set to create the final angiogram. Like any subtraction-based technique, the requirement of two scans increases scan time. Typical total scan times are similar to cardiac-gated 3D FSE NCE-MRA at 3 to 4 minutes. The FSD module is typically appended to a flow-compensated sequence like bSSFP so the total flow-spoiling effect is dominated by the choice of m1 and not the readout sequence itself. Like cardiac-gated 3D FSE NCE-MRA, FSD commonly uses a 3D acquisition to acquire good slice resolution by acquiring in a coronal orientation.

Since all flowing spins produce a signal difference in the BA-DA subtraction of FSD, venous signal can also appear in the final subtracted angiogram. The amount of venous contamination can be controlled by selecting an optimal value of m1 (69). High m1 generates a strong signal difference between BA and DA scans, thus generating bright arterial signal in the angiogram. However, a high m1 also produces a large signal difference between BA and DA scans in veins, resulting in venous contamination. A low m1 only weakly dephases the slowly flowing venous spins in the DA scan, resulting in little venous contamination in the angiogram. But a low m1 reduces the signal difference between BA and DA scans for arteries, particularly slow-flowing arteries, resulting in a loss of arterial signal in the angiogram. Therefore, m1 needs to be calibrated based on a trade-off between arterial signal loss and venous contamination (69).

The primary advantage of FSD is the high vessel signal in the BA scan. Since the bSSFP readout method is flow-compensated, all vessels are well-depicted in the BA scan, regardless of velocity. In comparison, the inherent flow-spoiling effect of the FSE readout in cardiac-gated 3D FSE NCE-MRA causes some arterial signal to be lost even in the BA scan, especially in vessels with fast-flowing blood. Compared to the FSE readout of cardiac-gated 3D FSE NCE-MRA, the bSSFP readout of FSD provides high SNR and sharp image resolution due to the lack of T2-blurring. This feature enables FSD to produce high-resolution angiograms particularly useful for depicting small vessels in feet and hands. The use of bSSFP requires good B_0 homogeneity. Thus, similar to QISS, the extent of applications is determined by the quality of static magnetic field (B_0) homogeneity. Therefore, the FSD technique may potentially struggle with large volume coverage or near areas with strong susceptibility fields (eg, lungs).

The flow-dephasing effect is related to the direction of blood flow relative to the direction of the flow-dephasing gradients. Thus, blood flow perpendicular to the flow-dephasing direction is not affected at all and does not appear in the FSD-generated angiogram. To address this orientation-sensitivity issue, at the

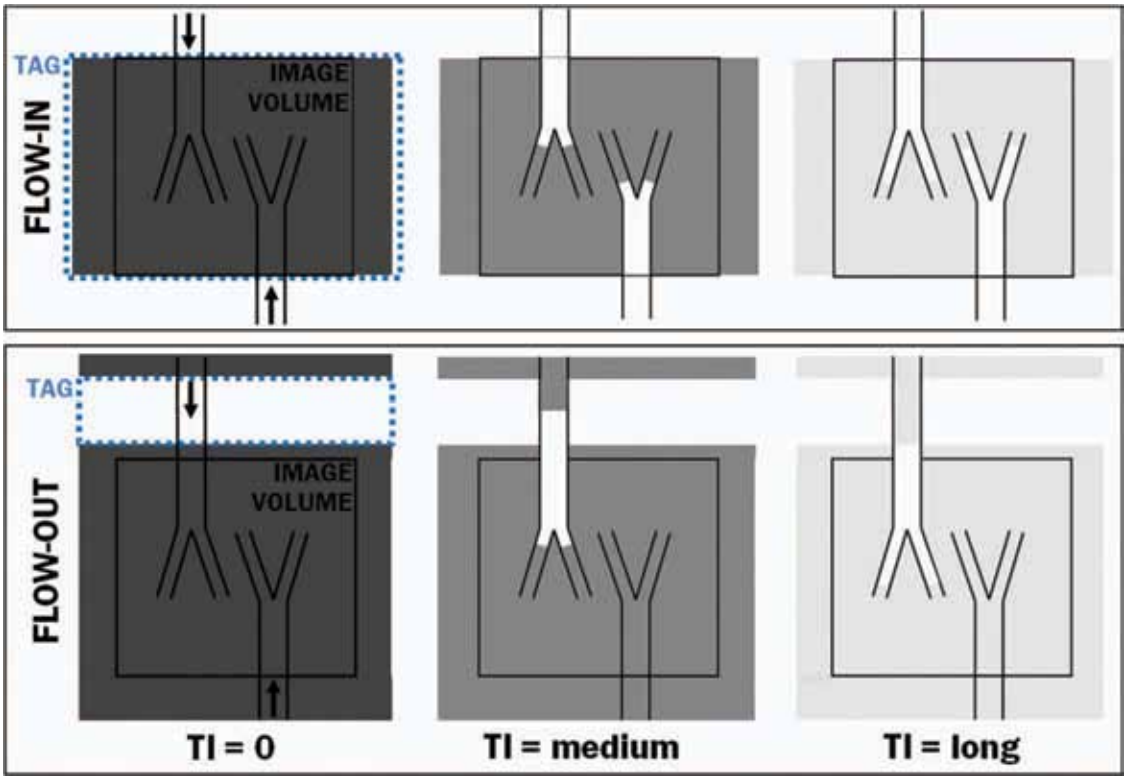

Figure 10. Illustration of flow-in and flow-out spin-labeling. The blue dotted box represents the selective tag region. The image volume (black box) is fed by two arteries. The direction of flow for each artery is indicated by arrows. The grayscale color represents longitudinal magnetization with white corresponding to positive ($M_z = 1$) and dark gray corresponding to negative ($M_z = -1$). Top row: Flow-in spin labeling. The tag region typically corresponds to the imaging volume, although they need not be identical. At TI = 0, all spins within the tag region are inverted. After medium TI, fresh magnetization from outside the tag has flowed into the vessels. At long TI, the blood has flowed into the distal branches. Stationary tissue signal has recovered by T1 relaxation, reducing contrast. Bottom row: Flow-out spin labeling. In this illustration, the tag region was drawn above the imaging volume. However, the tag region can be selected, rotated, and positioned independent of the imaging volume. At TI = 0, only the tagged region contains positive longitudinal magnetization; all other magnetization is inverted. At medium TI, blood has flowed out of the tag region and into the imaging volume. Only the vessel fed with tagged blood is depicted in the image. At long TI, blood has flowed into the distal branches of the tagged vessel while stationary tissue signal has recovered.

cost of SNR loss due to T2 decay, additional FSD modules with orthogonal flow-dephasing directions can be included. For example, FSD modules with bipolar gradients on the RO axis and PE axis can be applied sequentially to dephase all in-plane blood flow (70).

Applications

The FSD technique has been applied to peripheral arteries using a single module with flow-dephasing in the craniocaudal direction (68,69,71). The total acquisition time for a 40-cm coverage is 3–4 minutes, similar to cardiac-gated 3D FSE NCE-MRA. Using the two-module approach, depiction of the tortuous vessels in the hand can be achieved (70). Figure 8 shows the application of the two-module approach to depict the small vasculature of the digital arteries in exquisite detail.

SPIN LABELING TECHNIQUES

General Mechanism of Spin Labeling

The general technique of arterial spin labeling (ASL) uses some form of a selective inversion pulse to label or "tag" the longitudinal magnetization of inflowing blood. This tag can be applied in many ways, but the fundamental purpose is to force the longitudinal magnetization of flowing blood to differ from that of stationary tissue. Following the tagging, an inversion recovery delay period (TI) allows blood to flow into the imaging slab, after which it is read out with a conventional sequence. Spin labeling can be applied using three methods: flow-in, flow-out, and tag-alternation. The names "flow-in" and "flow-out" are in reference to the flow direction relative to the selective tag. Figure 9 illustrates the basic pulse sequence for each method. A pictogram of the typical flow-in and flow-out tag placements is provided in Figure 10.

Flow-In Spin Labeling Method

Description

In the flow-in method, the tagging pulse is applied to the entire imaging slab (Fig. 10). The tag inverts both blood and stationary spins in the region of interest. During the TI, fresh inflowing blood enters the imaging slab while the spins in stationary tissue and blood preexisting in the imaging volume return toward null

Figure 11. Example of renal NCE-MRA using flow-in spin labeling. Coronal MIP image of a 37-year-old healthy volunteer. The image was acquired using the flow-in technique with a spatially selective IR pulse applied to a volume containing the kidneys. A presaturation pulse was applied inferior to the renal region to achieve venous suppression.

magnetization ($M_z \approx 0$) via T1 recovery (Fig. 9a). The imaging slab is then read out using any conventional sequence. The fresh inflowing blood is depicted with bright signal due to its full amplitude longitudinal magnetization. If the TI approximately matches the null point of stationary tissue, the background signal is dark. These techniques are available under the commercial trade names of time-SLIP, NATIVE true-FISP, Inflow-IR, and b-TRANCE.

Applications

The most common clinical application of flow-in spin labeling NCE-MRA is renal angiography. The complex orientations of the aorta and renal arteries dictate the use of bSSFP due to its inherent multidirectional flow-compensation. The flow-in method is commonly used with a tag over the kidneys (Fig. 11). Flow-in spin labeling in conjunction with a respiratory real-time motion correction technique has been used to depict the renal arteries (72). Renal flow-in spin labeling NCE-MRA has been compared to CTA (73) and DSA (74,75) in several clinical studies. Similar to other NCE-MRA techniques, the clinical comparison studies (73–75) report high sensitivity (100%, 100%, and 93%, respectively) but lower specificity (93%, 88%, and 88%, respectively) for flow-in spin labeling versus

Figure 12. Example of the flow-out spin labeling method used for time-resolved NCE-MRA of the left carotid artery. Shown are MIP projections for TI from 400 msec to 1200 msec. Note that as the TI increases, stationary tissue signal starts to recover. (Image courtesy of Y. Yamashita and T. Yamamoto of Toshiba Medical Systems Corp., Tochigi, Japan.)

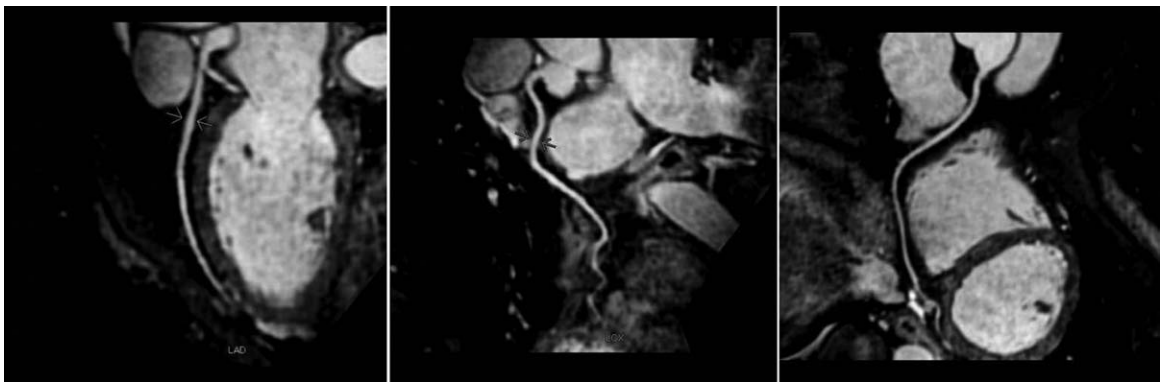

Figure 13. Example of bSSFP angiography of the coronary arteries in a 39-year-old female volunteer. Left: left anterior descending (LAD) coronary artery. Middle: left circumflex (LCX) coronary artery. Right: right coronary artery (RCA). (Image courtesy of Dr. Y. Ohmoto and staff of Radiology Department, Toranomon Hospital, Toyko, Japan.)

conventional radiology methods, indicating the potential of spin labeling NCE-MRA as a diagnostic screening test.

Flow-Out Spin Labeling Method

Description

The flow-out method applies the tagging pulse upstream on a vessel of interest (Fig. 10). The selective tagging pulse is immediately preceded by a nonselective inversion pulse (Fig. 9b). The nonselective pulse first inverts all longitudinal magnetization, including the stationary tissue and preexisting blood in the imaging slab. The tag pulse selectively restores the magnetization of the upstream tagged blood to positive longitudinal magnetization ($M_z \approx 1$) while leaving the longitudinal magnetization in the stationary tissue inverted. The process unfolds much like flow-in spin labeling; during the TI, tagged blood with full magnetization flows out of the tag region and into the imaging volume while the magnetization of stationary tissue returns toward null via T1 recovery. Like the flow-in method, the background signal is dependent on the chosen TI and stationary tissue T1.

Applications

Flow-out spin labeling has been used to depict vessels in and around the liver including hepatic arteries (76), hepatic veins (77), and the portal system (78). To depict the hepatic veins, double tag pulses were applied with one tag positioned on the upper liver to suppress signals from the aorta, and the other tag positioned below the liver to suppress signals from the portal veins (77). To depict the portal system, double tag pulses were also used (78). One tag covered the liver and thorax simultaneously to provide suppression of background signal from liver and myocardium as well as suppress inflowing blood from the hepatic arterial system. The other tag was positioned below the liver to suppress ascending venous blood signal from the inferior vena cava to avoid overlap with the signal from the portal vein. The effect of food intake on the portal system has also been studied using flow-out spin labeling (79). Another application of a 2D flow-out technique shows bulk flow movement of cerebrospinal fluid in the intracranial and intraspinal compartments (80).

Tag-Alternation Spin Labeling Method

Description

The tag-alternation method is the most standard form of spin labeling. The method can be applied in many forms, but the general concept is to acquire two scans in an alternated fashion: a tag image with upstream tagging of arterial blood and a control image without tagging (81) (Fig. 9c). The subtraction of the two image sets removes signal from stationary tissue and leaves only the tagged spins in the resultant angiogram.

The tag application can be achieved with several approaches. The tag can be applied with a selective upstream tagging pulse that is alternated on-off in the corresponding tag-control scans. This general method is used for time-SLIP (82), STAR (83), STARFIRE (84), and EPISTAR (85) techniques.

Applications

Tag-alternation spin labeling can be used for pulmonary angiography using a sagittal selective tag placed over the heart. During the TI, the blood flows out of the tag and into the lungs, where it is later read out using a 2D FSE (86) or 3D gradient-echo (87) sequence. The portal system has been studied using the tag-alternation method where both tag-on and tag-off images were acquired in a single breath-hold (88). Tag-alternation spin labeling can be used in carotid angiography with a tag applied over the heart (84). Since spin labeling NCE-MRA is not hindered by the limitations of inflow effects, it is able to depict flow in the carotid notch and bulb. An example of a time-resolved application in the left carotid artery is depicted in Figure 12.

General Considerations for Spin Labeling Methods

In the flow-in method, only blood that flows into the tag region (which corresponds to the imaging slab) is visible. This inflowing blood can come from any

Table 1
Summary of NCE-MRA Methods

Class	Method	Primary applications	Typical scan time	Vessel orientation	Stationary tissue/ venous signal background contamination
Inflow-based	3D TOF	Intracranial extracranial carotids	5 min per brain	Vessels perpendicular to slices	Moderate stationary tissue signal, Some venous (removed by segmentation)
	HOP-MRA	Intracranial	5 min per brain	Vessels perpendicular to slices	Little to none
	2D TOF	Peripheral extracranial carotids	4 min per coverage, 20 min per calf station	Vessels perpendicular to slices	Little stationary tissue signal, Some venous (removed by segmentation)
	QISS	Peripheral	1-2 min per coverage, 8-10 min iliac to calf station	Vessels perpendicular to slices	Little to none
Cardiac-phase-dependent	Cardiac-Gated 3D FSE	Pulmonary, aortic, hepatic, peripheral, extremity	3-4 min per coverage, 10-12 min liac to calf station	Vessels parallel to readout preferred	None
Flow-encoding	2D/3D PC-MRA	Flow quantification	Depends on number of PC directions	Depends on number of PC directions	No stationary tissue signal, some venous (removed by segmentation)
	4D Flow	Flow quantification, flow dynamics	10-20 min	Any	No stationary tissue signal, some venous (removed by segmentation)
	FSD	Upper and lower extremity	3-4 min per coverage	Depends on number of FSD directions	No stationary tissue signal, some venous signal
Spin labeling	Flow-In	Renal, hepatic	2 min	Any	Moderate stationary tissue signal - depends on TI
	Flow-Out	Pulmonary, CSF, carotid, hepatic	2 min	Any	Moderate stationary tissue signal - depends on TI
	Tag-Alternation	Pulmonary, carotid, CSF, extremity	3-4 min per TI increment	Any	None
Relaxation	bSSFP	Coronary, renal, extremity	14 min per whole heart volume (navigator gated, free breathing)	Any	Moderate stationary tissue signal – depends on use of T2 preparation and/or inversion recovery

supply source. In situations where an organ is fed by multiple sources, like the portal vein, which receives blood from both the splenic and the superior mesenteric veins, the relative contributions of each source vessel cannot be determined using the flow-in approach. Therefore, the flow-in method is most applicable to angiography applications. In the flow-out method, only blood selected by the finite tag region is visible. Therefore, the flow depiction can be isolated to distinct vessels. The flow-out method allows the supply functionality aspects of individual vessels to be analyzed. In the tag-alternation method, a selective tagging approach is used and hence its flow selectivity characteristics are the same as the flow-out method.

Since the flow-in method depicts inflow from any source, venous signal can also appear in the imaging slab. To further suppress venous inflow, a spatial presaturation pulse can be applied over the venous source. For example, in renal applications of flow-in spin labeling, an axial presaturation slab is commonly placed inferior to the imaging volume to suppress venous inflow from the inferior vena cava.

Although all three spin labeling methods can be used with any conventional data acquisition sequence, they usually are used with either 3D bSSFP or 3D FSE acquisition methods. Naturally, 2D acquisition is available, but like other NCE-MRA methods, the 3D acquisition is used to achieve good slice resolution. In general, the high resolution and flow-compensation of bSSFP makes it the method of choice for most applications except for pulmonary arteries and subclavian vessels near the air–tissue interface of the lungs, where FSE is preferred. Although spin-labeling techniques can be cardiac-gated if it is appropriate for the application, spin labeling does not require cardiac-gating like the cardiac-phase-dependent class of NCE-MRA methods.

The flow-in and flow-out techniques require careful selection of the TI with respect to the flow velocity in the vessel of interest and the T1 of stationary tissue. Ideally, the TI is chosen to correspond to the null point of the stationary tissue. However, if flow is slow, a longer TI might be required for good vessel depiction at the cost of increased background signal. Thus, the flow-in and flow-out techniques are best suited for applications where blood velocity is fast relative to TI. The removal of signal from stationary tissue via subtraction using the tag-alternation method avoids the dependency on TI. Therefore, the tag-alternation method can be applied for even arteries with slow-flowing blood like those in the distal extremities. Since the spin-labeling methods can be used across a range of TI, they can be used to acquire time-resolved NCE-MRA data. By incrementally adjusting TI for N repeated acquisitions, blood flow dynamics can be depicted. Since the TI can be freely selected for each of the N images, the time increment using this approach can be arbitrarily small. However, in practice, the time range and resolution is bounded by the scan time burden of N (or Nx2 in the case of tag-alternation) acquisitions. The maximum TI is bounded by the tag persistence, which decays with the T1 of tagged blood.

RELAXATION-BASED TECHNIQUES

General Mechanism of Using Relaxation for NCE-MRA

The fundamental differences in relaxation between arterial, venous, and adjacent stationary tissue can be leveraged to generate angiograms. The T2 and T2* of venous blood is shorter than that arterial blood due to the reduced oxygenation of hemoglobin (22,23). In general, the T1 of adjacent stationary tissues, whether muscles or organs, is shorter than that of blood, since blood consists of a higher percentage of free water (22). Arterial signal can be selectively depicted, and venous and stationary tissue signals relatively suppressed, using one or more approaches based on T2/T1-, T2-, T2*-, or T1-weighted contrast without the explicit removal the stationary tissue signal using saturation, subtraction, or inversion recovery mechanisms as in other NCE-MRA methods. Since the vessel depiction is independent of flow velocity, orientation, or dependency on cardiac cycle, these techniques are often referred to as "flow-independent."

The relaxation-based approach fundamentally relies on venous and surrounding stationary tissue signals decaying faster than arterial signals. Thus, these approaches result in some collateral arterial signal loss. Therefore, relaxation-based NCE-MRA must trade-off between improving the quality of suppression at the cost of arterial signal loss. In practice, signals from stationary tissue and veins are nonzero as they would be with subtraction-based methods. But depending on the application, perfect background suppression is not necessary if the vessels of interest are adequately conspicuous.

bSSFP

Technique

With the proper sequence parameter selection, the T2/T1-weighted contrast and inherent flow-compensation of bSSFP generally makes signal from stationary tissue relatively dark compared to the bright signals from the vessels. In this way, bSSFP can be used by itself as an NCE-MRA method. The bSSFP sequence depicts all blood in the imaging slab regardless of its source or flow velocity. Therefore, venous signal appears in the bSSFP images alongside arterial signal. To enhance arterial depiction, an inversion recovery pulse coupled with a T2-preparation prepulse (basically an FSD module without the flow-encoding gradients) can be used to suppress adjacent tissue and veins while leaving arterial signal mostly intact (89,90). Often, fat signal appears bright in bSSFP images. Therefore, some form of fat suppression is typically employed to increase vessel-to-background contrast.

Applications

The multidirectional flow-compensation of bSSFP makes the technique a good candidate for imaging the renal arteries. Two clinical studies comparing breath-hold bSSFP NCE-MRA with DSA (91) and CE-MRA

(92) in the detection of renal stenoses reported strong potential for bSSFP as a screening test with sensitivities of 100% and 92%, respectively, and specificities of 98% and 81%, respectively. Another clinical study reported significant improvement in image quality using respiratory navigator-gated bSSFP NCE-MRA instead of the breath-hold approach (93). The Dixon method bSSFP, where two bSSFP images acquired with different center frequency offsets are combined using the Dixon method (94), has been demonstrated to depict conspicuous vessels with good fat suppression for NCE-MRA in renal arteries (95) and arteries of the extremities (96). Also leveraging the frequency selectivity of bSSFP, fat-suppressed bSSFP NCE-MRA can be used in conjunction with an alternate TR bSSFP technique to reduce fat signal to image the arteries in the lower extremities (97).

Due to the very fast flow and lack of substantial fat or venous vasculature, bSSFP is particularly applicable to NCE-MRA in and around the heart. A common application of bSSFP is coronary NCE-MRA (98). By incorporating thin-slab 3D bSSFP with ECG-gating and breath-holding, high-resolution angiograms of the coronary arteries can be obtained (Fig. 13). More recently, free-breathing navigator-gated, whole-heart NCE-MRA has been successfully used to acquire volumetric image sets (99). The whole-heart image volume data can be repeatedly reformatted to deliver the best depiction of each vessel, which is especially useful given the curvature of the coronary arteries. Another common application of bSSFP NCE-MRA is imaging the thoracic aorta (100). The inherent flow-compensation of bSSFP is able to capture the fast arterial flow in the aorta.

SUMMARY

NCE-MRA has been demonstrated in a wide variety of cardiovascular applications including brain, heart, lungs, liver, kidneys, hands, and lower extremities. The proper NCE-MRA method for each application depends on the anatomy and characteristics of the vessels of interest. In the above discussion, established and emerging methods are compared and contrasted with regard to their features and limitations. Table 1 summarizes these techniques and their intended primary applications.

REFERENCES

1. Prince MR. Gadolinium-enhanced MR aortography. Radiology 1994;191:155–164.
2. Wilman AH, Riederer SJ, King BF, Debbins JP, Rossman PJ, Ehman RL. Fluoroscopically triggered contrast-enhanced three-dimensional MR angiography with elliptical centric view order: application to the renal arteries. Radiology 1997;205:137–146.
3. Kita M, Mitani Y, Tanihata H, et al. Moving-table reduced-dose gadolinium-enhanced three-dimensional magnetic resonance angiography: velocity-dependent method with three-phase gadolinium infusion. J Magn Reson Imaging 2001;14:319–328.
4. Ho KY, Leiner T, de Haan MW, Kessels AG, Kitslaar PJ, van Engelshoven JM. Peripheral vascular tree stenoses: evaluation with moving-bed infusion-tracking MR angiography. Radiology 1998;206:683–692.
5. Urata J, Miyazaki M, Wada H, Nakaura T, Yamashita Y, Takahashi M. Clinical evaluation of aortic diseases using nonenhanced MRA with ECG-triggered 3D half-Fourier FSE. J Magn Reson Imaging 2001;14:113–119.
6. Sadowski EA, Bennett LK, Chan MR, et al. Nephrogenic systemic fibrosis: risk factors and incidence estimation. Radiology 2007;243:148–157.
7. Roditi G, Maki JH, Oliveira G, Michaely HJ. Renovascular imaging in the NSF era. J Magn Reson Imaging 2009;30:1323–1334.
8. Moreno-Romero JA, Segura S, Mascaro JMJr, et al. Nephrogenic systemic fibrosis: a case series suggesting gadolinium as a possible aetiological factor. Br J Dermatol 2007;157:783–787.
9. Clorius S, Technau K, Watter T, et al. Nephrogenic systemic fibrosis following exposure to gadolinium-containing contrast agent. Clin Nephrol 2007;68:249–252.
10. Khurana A, Runge VM, Narayanan M, Greene JFJr, Nickel AE. Nephrogenic systemic fibrosis: a review of 6 cases temporally related to gadodiamide injection (Omniscan). Invest Radiol 2007;42:139–145.
11. Collidge TA, Thomson PC, Mark PB, et al. Gadolinium-enhanced MR imaging and nephrogenic systemic fibrosis: retrospective study of a renal replacement therapy cohort. Radiology 2007; 245:168–175.
12. Kuo PH, Kanal E, Abu-Alfa AK, Cowper SE. Gadolinium-based MR contrast agents and nephrogenic systemic fibrosis. Radiology 2007;242:647–649.
13. U.S. Food and Drug Administration. Gadolinium based contrast agents for magnetic resonance imaging (marketed as Magnevist, MultiHance, Omniscan, OptiMARK, ProHance). Rockville, MD: FDA, 2007.
14. Dawson P. Nephrogenic systemic fibrosis: possible mechanisms and imaging management strategies. J Magn Reson Imaging 2008;28:797–804.
15. Prince MR, Zhang HL, Roditi GH, Leiner T, Kucharczyk W. Risk factors for NSF: a literature review. J Magn Reson Imaging 2009;30:1298–1308.
16. Sodickson DK, Manning WJ. Simultaneous acquisition of spatial harmonics (SMASH): fast imaging with radiofrequency coil arrays. Magn Reson Med 1997;38:591–603.
17. Pruessmann KP, Weiger M, Scheidegger MB, Boesiger P. SENSE: sensitivity encoding for fast MRI. Magn Reson Med 1999;42: 952–962.
18. Miyazaki M, Lee VS. Nonenhanced MR angiography. Radiology 2008;248:20–43.
19. Morita S, Masukawa A, Suzuki K, Hirata M, Kojima S, Ueno E. Unenhanced MR angiography: techniques and clinical applications in patients with chronic kidney disease. Radiographics 2011;31:E13–E33.
20. Mizayaki M, Isoda H. Non-contrast-enhanced MR angiography of the abdomen. Eur J Radiol 2011;80:9–23.
21. Kanda T, Nakamura E, Moritani T, Yamori Y. Arterial pulse wave velocity and risk factors for peripheral vascular disease. Eur J Appl Physiol 2000;82:1–7.
22. Barth M, Moser E. Proton NMR relaxation times of human blood samples at 1.5 T and implications for functional MRI. Cell Mol Biol 1997;43:783–791.
23. Wright GA, Hu BS, Macovski A. Estimating oxygen saturation of blood in vivo with MR imaging at 1.5 T. J Magn Reson Imaging 1991;1:275–283.
24. Ono A, Murase K, Taniguchi T, et al. Deep vein thrombosis using non-contrast-enhanced MR venography with electrocardiographically-gated three-dimensional half-Fourier FSE: preliminary experience. Magn Reson Med 2009;61:907–917.
25. Masaryk TJ, Laub GA, Modic MT, Ross JS, Haacke EM. Carotid-CNS MR flow imaging. Magn Reson Med 1990;14:308–314.
26. Laub GA. Time-of-flight method of MR angiography. Magn Reson Imaging Clin N Am 1995;3:391–398.
27. Parker DL, Yuan C, Blatter DD. MR angiography by multiple thin slab 3D acquisition. Magn Reson Med 1991;17:434–451.
28. Blatter DD, Parker DL, Robinson RO. Cerebral MR angiography with multiple overlapping thin slab acquisition. Radiology 1991; 179:805–811.
29. Atkinson D, Brant-Zawadzki M, Gillan G, Purdy D, Laub G. Improved MR angiography: magnetization transfer suppression with variable flip angle excitation and increased resolution. Radiology 1994;190:890–894.
30. Pike GB, Hu BS, Glover GH, Enzmann DR. Magnetization transfer time-of-flight magnetic resonance angiography. Magn Reson Med 1992;25:372–379.

31. Edelman RR, Ahn SS, Chien D, et al. Improved time-of-flight MR angiography of the brain with magnetization transfer contrast. Radiology 1992;184:395–399.
32. Dagirmanjian A, Ross JS, Obuchowski N, et al. High resolution, magnetization transfer saturation, variable flip angle, time-of-flight MRA in the detection of intracranial vascular stenoses. J Comput Assist Tomogr 1995;19:700–706.
33. Oelerich M, Lentschig MG, Zunker P, Reimer P, Rummeny EJ, Schuierer G. Intracranial vascular stenosis and occlusion: comparison of 3D time-of-flight and 3D phase-contrast MR angiography. Neuroradiology 1998;40:567–573.
34. Korogi Y, Takahashi M, Mabuchi N, et al. Intracranial aneurysms: diagnostic accuracy of three-dimensional, Fourier transform, time-of-flight MR angiography. Radiology 1994;193:181–186.
35. White PM, Teasdale EM, Wardlaw JM, Easton V. Intracranial aneurysms: CT angiography and MR angiography for detection-prospective blinded comparison in a large patient cohort. Radiology 2001;219:739–749.
36. Willinek WA, Born M, Simon B, et al. Time-of-flight MR angiography: comparison of 3.0-T imaging and 1.5-T imaging—initial experience. Radiology 2003;229:913–920.
37. Kimura T, Ikedo M, Takemoto S. Hybrid of opposite-contrast MR angiography (HOP-MRA) combining time-of-flight and flow-sensitive black-blood contrasts. Magn Reson Med 2009;62:450–458.
38. Kimura T, Ikedo M, Takemoto S. Phase enhancement for time-of-flight and flow-sensitive black-blood MR angiography. Magn Reson Med 2011;66:437–447.
39. Tsuchiya K, Kobayashi K, Nitatori T, et al. Hybrid of opposite-contrast MRA of the brain by combining time-of-flight and black-blood sequences: initial experience in major trunk stenoocclusive diseases. J Magn Reson Imaging 2010;31:56–60.
40. Ersoy H, Zhang H, Prince MR. Peripheral MR angiography. J Cardiovasc Magn Reson 2006;8:517–528.
41. Kaufman JA, McCarter D, Geller SC, Waltman AC. Two-dimensional time-of-flight MR angiography of the lower extremities: artifacts and pitfalls. AJR Am J Roentgenol 1998;171:129–135.
42. Offerman EJ, Hodnett PA, Edelman RR, Koktzoglou I. Nonenhanced methods for lower-extremity MRA: a phantom study examining the effects of stenosis and pathologic flow waveforms at 1.5T. J Magn Reson Imaging 2011;33:401–408.
43. Heiserman JE, Drayer BP, Fram EK, et al. Carotid artery stenosis: clinical efficacy of two-dimensional time-of flight MR angiography. Radiology 1992;182:761–768.
44. Edelman RR, Sheehan JJ, Dunkle E, Schindler N, Carr J, Koktzoglou I. Quiescent-interval single-shot unenhanced magnetic resonance angiography of peripheral vascular disease: technical considerations and clinical feasibility. Magn Reson Med 2010; 63:951–958.
45. Jara H, Yu BC, Caruthers SD, et al. Voxel sensitivity function description of flow-induced signal loss in MR imaging: implications for black-blood MR angiography with turbo spin-echo sequences. Magn Reson Med 1999;41:575–590.
46. Axel L, Morton D. MR flow imaging by velocity-compensated/uncompensated difference images. J Comput Assist Tomogr 1987;11:31–34.
47. Hinks RS, Constable RT. Gradient moment nulling in fast spin echo. Magn Reson Med 1994;32:698–706.
48. Constable RT, Gore JC. The loss of small objects in variable TE imaging: implications for FSE, RARE, and EPI. Magn Reson Med 1992;28:9–24.
49. Miyazaki M, Ichinose N, Sugiura S, Kassai Y, Kanazawa H, Machida Y. A novel MR angiography technique: swap phase encode extended data (SPEED) acquisition using half-Fourier RARE. J Magn Reson Imaging 1998;8:505–507.
50. Wedeen VJ, Meuli RA, Edelman RR, et al. Projective imaging of pulsatile flow with magnetic resonance. Science 1985;230: 946–948.
51. Meuli RA, Wedeen VJ, Geller SC, et al. MR gated subtraction angiography: evaluation of lower extremities. Radiology 1986;159: 411–418.
52. Miyazaki M, Sugiura S, Tateishi F, Wada H, Kassai Y, Abe H. Non-contrast-enhanced MR angiography using 3D ECG-synchronized half-Fourier fast spin echo. J Magn Reson Imaging 2000;12:776–783.
53. Miyazaki M, Takai H, Sugiura S, Wada H, Kuwahara R, Urata J. Peripheral MR angiography: separation of arteries from veins with flow-spoiled gradient pulses in electrocardiography-triggered three-dimensional half-Fourier fast spin-echo imaging. Radiology 2003;227:890–896.
54. Nakamura K, Miyazaki M, Kuroki K, Yamamoto A, Hiramine A, Admiraal-Behloul F. Non-contrast-enhanced peripheral MRA: technical optimization of flow-spoiled fresh blood imaging for screening peripheral arterial diseases. Magn Reson Med 2011; 65:595–602.
55. Storey P, Atanasova IP, Lim RP, et al. Tailoring the flow sensitivity of fast spin-echo sequences for noncontrast peripheral MR angiography. Magn Reson Med 2010;64:1098–1108.
56. Lim RP, Hecht EM, Xu J, et al. 3D Non-gadolinium enhanced ECG-gated MRA of the distal lower extremities: preliminary clinical experience. J Magn Reson Imaging 2008;28:181–189.
57. Haneder S, Attenberger UI, Riffel P, Henzler T, Schoenberg SO, Michaely HJ. Magnetic resonance angiography (MRA) of the calf station at 3.0T: intraindividual comparison of non-enhanced ECG-gated flow-dependent MRA, continuous table movement MRA and time-resolved MRA. Eur Radiol 2011;21:1452–1461.
58. Lim RP, Storey P, Atanasova IP, et al. Three-dimensional electrocardiographically gated variable flip angle FSE imaging for MR angiography of the hands at 3.0 T: initial experience. Radiology 2009;252:874–881.
59. Dumoulin CL, Souza SP, Walker MF, Wagle W. Three-dimensional phase contrast angiography. Magn Reson Med 1989;9: 139–149.
60. Dumoulin CL, Yucel EK, Vock P, et al. Two- and three-dimensional phase contrast MR angiography of the abdomen. J Comput Assist Tomogr 1990;14:779–784.
61. Dumoulin CL. Phase contrast MR angiography techniques. Magn Reson Imaging Clin N Am 1995;3:399–411.
62. Prince MR, Schoenberg SO, Ward JS, et al. Hemodynamically significant atherosclerotic renal artery stenosis: MR angiographic features. Radiology 1997;205:128–136.
63. Iseda T, Nakano S, Miyahara D, Uchinokura S, Goya T, Wakisaka S. Poststenotic signal attenuation on 3D phase-contrast MR angiography: a useful finding in haemodynamically significant carotid artery stenosis. Neuroradiology 2000;42:868–873.
64. Markl M, Kilner PJ, Ebbers T. Comprehensive 4D velocity mapping of the heart and great vessels by cardiovascular magnetic resonance. J Cardiovasc Magn Reson 2011;13:7.
65. Markl M, Wallis W, Brendecke S, Simon J, Frydrychowicz A, Harloff A. Estimation of global aortic pulse wave velocity by flow-sensitive 4D MRI. Magn Reson Med 2010;63:1575–1582.
66. Harloff A, Nussbaumer A, Bauer S, et al. In vivo assessment of wall shear stress in the atherosclerotic aorta using flow-sensitive 3D MRI. Magn Reson Med 2010;63:1529–1536.
67. Harloff A, Simon J, Brendecke S, et al. Complex plaques in the proximal descending aorta: an underestimated embolic source of stroke. Stroke 2010;41:1145–1150.
68. Fan Z, Sheehan J, Bi X, Liu X, Carr J, Li D. 3D noncontrast MR angiography of the distal lower extremities using flow-sensitive dephasing (FSD)-prepared balanced SSFP. Magn Reson Med 2009;62:1523–1532.
69. Fan Z, Zhou X, Bi X, Dharmakumar R, Carr J, Li D. Determination of optimal first-order gradient moment for flow-sensitive dephasing magnetization-prepared 3D noncontrast MR angiography. Magn Reson Med 2011;65:964–972.
70. Sheehan JJ, Fan Z, Davarpanah AH, et al. Nonenhanced MR angiography of the hand with flow-sensitive dephasing-prepared balanced SSFP sequence: initial experience with systemic sclerosis. Radiology 2011;259:248–256.
71. Priest AN, Graves MJ, Lomas DJ. Non-contrast-enhanced vascular magnetic resonance imaging using flow-dependent preparation with subtraction. Magn Reson Med 2012;67:628–637.
72. Spuentrup E, Manning WJ, Bornert P, Kissinger KV, Botnar RM, Stuber M. Renal arteries: navigator-gated balanced fast field-echo projection MRA with aortic spin labeling: initial experience. Radiology 2002;225:589–596.
73. Wyttenbach R, Braghetti A, Wyss M, et al. Renal artery assessment with nonenhanced steady-state free precession versus contrast-enhanced MR angiography. Radiology 2007;245:186–195.
74. Lanzman RS, Voiculescu A, Walther C, et al. ECG-gated nonenhanced 3D steady-state free precession MR angiography in assessment of transplant renal arteries: comparison with DSA. Radiology 2009;252:914–21.
75. Parienty I, Rostoker G, Jouniaux F, Piotin M, Admiraal-Behloul F, Miyazaki M. Renal artery stenosis evaluation in chronic

kidney disease patients: nonenhanced time-spatial labeling inversion-pulse three-dimensional MR angiography with regulated breathing versus DSA. Radiology 2011;259:592–601.
76. Shimada K, Isoda H, Okada T, et al. Non-contrast-enhanced hepatic MRA with true steady-state free-precession and time spatial labeling inversion pulse: optimization of the technique and preliminary results. Eur J Radiol 2009;70:111–117.
77. Shimada K, Isoda H, Okada T, et al. Non-contrast-enhanced MRA for selective visualization of the hepatic vein and inferior vena cava with true steady-state free-precession sequence and time-spatial labeling inversion pulses: preliminary results. J Magn Reson Imaging 2009;29:474–479.
78. Shimada K, Isoda H, Okada T, et al. Non-contrast-enhanced MR portography with time-spatial labeling inversion pulses: comparison of imaging with three-dimensional half-Fourier fast spin-echo and true steady-state free-precession sequences. J Magn Reson Imaging 2009;29:1140–1146.
79. Tsukuda T, Ito K, Koike S, Sasaki et al. Pre- and postprandial alterations of portal venous flow: evaluation with single breath-hold three-dimensional half-Fourier fast spin-echo MR imaging and a selective inversion recovery tagging pulse. J Magn Reson Imaging 2005;22:527–533.
80. Yamada S, Miyazaki M, Kanazawa H, et al. MRI visualization of cerebrospinal fluid movement with spin labeling: preliminary results in normal and pathophysiological conditions. Radiology 2008;249:644–652.
81. Nishimura DG, Macovski A, Pauly JM, Conolly SM. MR angiography by selective inversion recovery. Magn Reson Med 1987;4: 193–202.
82. Kanazawa H, Miyazaki M.Time-spatial labeling inversion tag (t-SLIT) using a selective IR-tag on/off pulse in 2D and 3D half-Fourier FSE as arterial spin labeling. In: Proc 10th Annual Meeting ISMRM, Honolulu; 2002. p140.
83. Edelman RR, Siewert B, Adamis M, Gaa J, Laub G, Wielopolski P. Signal targeting with alternating radiofrequency (STAR) sequences: application to MR angiography. Magn Reson Med 1994;31:233–238.
84. Koktzoglou I, Edelman RR. Star and STARFIRE for flow-dependent and flow-independent noncontrast carotid angiography. Magn Reson Med 2009;61:117–124.
85. Edelman RR, Chen Q. EPISTAR MRI: multislice mapping of cerebral blood flow. Magn Reson Med 1998;40:800–805.
86. Mai VM, Berr SS. MR perfusion imaging of pulmonary parenchyma using pulsed arterial spin labeling techniques: FAIRER and FAIR. J Magn Reson Imaging 1999;9:483–487.
87. Mai VM, Hagspiel KD, Altes T, Goode AR, Williams MB, Berr SS. Detection of regional pulmonary perfusion deficit of the occluded lung using arterial spin labeling in magnetic resonance imaging. J Magn Reson Imaging 2000;11:97–102.
88. Ito K, Shimizu A, Tsukada T, et al. Evaluation of intraportal venous flow distribution by unenhanced MR angiography using three-dimensional fast spin-echo with a selective tagging pulse: efficacy of subtraction of tag-on and tag-off images acquired during a single breath-hold. J Magn Reson Imaging 2009;29: 1224–1229.
89. Brittain JH, Hu BS, Wright GA, Meyer CH, Macovski A, Nishimura DG. Coronary angiography with magnetization-prepared T2 contrast. Magn Reson Med 1995;33:689–696.
90. Shea SM, Deshpande VS, Chung YC, Li D. Three-dimensional true-FISP imaging of the coronary arteries: improved contrast with T2-preparation. J Magn Reson Imaging 2002;15:597–602.
91. Coenegrachts K, Hoogeveen R, Vaninbroukx J, et al. High-spatial resolution 3D balanced turbo field-echo technique for MR angiography of the renal arteries: initial experience. Radiology 2004;231:237–242.
92. Herborn C, Watkins D, Runge V, Gendron J, Montgomery M, Naul L. Renal arteries: comparison of steady-state free precession MR angiography and contrast-enhanced MR angiography. Radiology 2006;239:263–268.
93. Maki JH, Wilson GJ, Eubank WB, Glickerman DJ, Pipavath S, Hoogeveen RM. Steady-state free precession MRA of the renal arteries: breath-hold and navigator-gated techniques vs. CE-MRA. J Magn Reson Imaging 2007;26:966–973.
94. Huang TY, Chung HW, Wang FN, Ko CW, Chen CY. Fat and water separation in balanced steady-state free precession using the Dixon method. Magn Reson Med 2004;51:243–247.
95. Stafford RB, Sabati M, Haakstad MJ, Mahallati H, Frayne R. Unenhanced MR angiography of the renal arteries with balanced steady-state free precession Dixon method. Am J Roentgenol 2008;191:243–246.
96. Stafford RB, Sabati M, Mahallati H, Frayne R. 3D non-contrast enhanced MR angiography with balanced steady-state free precession Dixon method. Magn Reson Med 2008;59:430–433.
97. Çukur T, Lee JH, Bangerter NK, Hargreaves BA, Nishimura DG. Non-contrast-enhanced flow-independent peripheral MR angiography with balanced SSFP. Magn Reson Med 2009;61: 1533–1539.
98. Deshpande VS, Shea SM, Laub G, Simonetti OP, Finn JP, Li D. 3D magnetization-prepared true-FISP: a new technique for imaging coronary arteries. Magn Reson Med 2001;46:494–502.
99. Sakuma H, Ichikawa Y, Suzawa N, et al. Assessment of coronary arteries with total study time of less than 30 minutes by using whole-heart coronary MR angiography. Radiology 2005;237: 316–321.
100. Amano Y, Takahama K, Kumita S. Non-contrast-enhanced MR angiography of the thoracic aorta using cardiac and navigator-gated magnetization-prepared three-dimensional steady-state free precession J Magn Reson Imaging 2008;27:504–509.

PRINTED HOME STUDY EDUCATIONAL SEMINARS

Qty.	Vol.	CE	Home Studies Title
	1.1	3.5	Functional MRI: Capabilities and Limitations
	1.2	3.0	Concepts in MR Physics
	2.1	3.5	Considerations in Low Field MRI
	2.2	3.0	Directions in Basic Cardiac Imaging
	2.3	3.0	Directions in Advanced Cardiac Imaging
	2.4	1.5	The Basics of Magnetic Resonance Angiography
	3.1	3.0	Introduction to Spectroscopy
	3.2	1.0	Renal MR Imaging
	3.3	3.0	A Primer on MR Pulse Sequences
	3.4	2.5	Artifacts Encountered in Abdominal MRI
	4.1	3.0	Safety Aspects in MRI
	4.2	3.0	Directions in MRI of the Liver
	4.3	2.0	MR Techniques in the Evaluation of the Uterus
	4.4	3.0	Fundamental Principles for MR Imaging of the Brain
	5.1	2.5	Atlas of Cranial Neuroanatomy
	5.2	2.0	MRI of the Ankle & Foot
	5.3	3.0	MR Imaging of the Breast
	5.4	1.0	Diffusion-Weighted Imaging of the Brain
	6.1	1.0	Directions in MRA of the Abdominal Aorta and Lower Extremities
	6.2	3.5	Fundamental Principles of MR Imaging of the Head, Neck, and Spine
	6.3	1.5	Advances in Interventional MRI
	6.4	1.5	Diffusion-Weighted MR Imaging of the Pediatric Brain
	7.1	2.0	The Role of Neuroimaging in the Diagnosis of Alzheimer's Disease
	7.2	2.5	Cardiovascular MRI: Update I
	7.3	2.5	K-Space in the Clinic
	7.4	3.0	MR Imaging and Spectroscopy of the Prostate
	8.1	1.0	Atlas of Knee Anatomy
	8.2	2.0	Cardiovascular MRI: Update II
	8.3	2.5	Update: Safety in MR Examinations
	8.4	2.0	Parallel MR Imaging

Qty.	Vol.	CE	Home Studies Title
	9.1	3.0	MRI of Breast Cancer: Update I
	9.2	2.5	MR Atlas of the Shoulder
	9.3	3.0	Exploring Magnetic Field Strengths: Challenges and Opportunities
	9.4	4.0	MRI of Breast Cancer: Update II
	10.1	4.0	MR Imaging of Perfusion
	10.2	3.0	MR Imaging Artifacts:Appearance, Cause & Cure
	10.3	4.0	Techniques in Cardiovascular MR Imaging
	10.4	3.0	MRI of the Brain
	11.1	4.0	Update: Musculoskeletal MRI*
	11.2	2.5	Contrast Media in MRI Examinations*
	11.3	2.0	Head and Neck MRI at 3.0T
	11.4	3.0	MR Imaging of the Abdomen*
	12.1	3.0	Contrast-Enhanced Musculoskeletal MR Imaging
	12.2	3.0	Neuro MRI: Principles and Protocols*
	12.3	2.0	MR Imaging of the Spine*
	12.4	3.0	MR Imaging of the Liver*
	13.1	3.0	MR Imaging Sequences: Gradient-Recalled Echo (GRE)*
	13.2	3.5	Techniques in Cardiac MR Imaging*
	13.3	2.5	Phase Contrast MR Imaging: Techniques and Applications*
	13.4	2.0	MRI of Spinal Cord Lesions*
	14.1	3.0	Breast MRI: DCIS and Skin Lesions*
	14.2	3.5	Pediatric Magnetic Resonance Imaging*
	14.3	2.5	MR Imaging Physics Tutorial*
	14.4	2.5	Safety and Screening in MRI*
	15.1	2.0	MR of the Abdomen: Kidney*
	15.2	2.5	3D Musculoskeletal MR Imaging*
	15.3	2.5	MR Physics: Gradient Echo & Parallel Imaging*
	15.4	1	MRI Atlas of the Abdomen*

All home study educational seminars following Volume 15.4 will be available ONLINE ONLY.

*Home Study Educational Seminars available online at no cost to SMRT members.

HOME STUDY EDUCATIONAL SEMINARS ORDER FORM

Back issues of SMRT educational seminars are for sale to SMRT members only!

YOU MAY ORDER PAST ISSUES OF HOME STUDY EDUCATIONAL SEMINARS ONLINE:

http://cds.ismrm.org/protected/ehs/hsorder.htm

TO ORDER BY MAIL, PLEASE FILL OUT AND MAIL THIS FORM, INCLUDING YOUR QUANTITY AND CHOICE OF ISSUES FROM PREVIOUS PAGE

CALCULATE YOUR ORDER HERE

Total quantity ordered: _____ x US$25 each = $_____ Subtotal = US$_____

SHIPPING:

Shipping is included on orders of four volumes or less. Shipping is charged on orders of five volumes or more. We will contact you with the shipping cost before we process your order. No orders will be processed before you have confirmed the actual shipping cost.

PAYMENT OPTIONS & BILLING INFORMATION

PAYMENT WITHIN USA:

Personal checks, money orders, cashier's checks and company checks are acceptable. Institutional purchase orders are acceptable and will be invoiced, but payment must still be received prior to shipment.

PAYMENT FROM OUTSIDE USA:

Checks: The check must be payable "to" (NOT "through") a U.S. bank in U.S. Dollars. The check must be imprinted with the computer encoding and routing information authorized by the American Banking Association.

Traveler's Checks: Traveler's checks in U.S. dollars for the exact amount, properly counter-signed, are acceptable.
International Money Order: The money order must be in U.S. dollars and be imprinted with the computer encoding and routing information authorized by the American Banking Association. U.S. dollar International Postal Money Orders imprinted as stated above are acceptable.

Wire: Wire payments are not accepted.

SMRT Member ID# (REQUIRED)_____

Name_____

Address_____

City_____State/Province_____Postal Code/ZIP + 4_____Country_____

Phone_____Fax_____E-mail_____

❒ Credit Card: ❒ VISA ❒ MasterCard ❒ AMEX ❒ Discover

(Credit card orders may be faxed directly to SMRT: +1 510 841 2340)

Card Number: _____Expiration Date:_____Security Code:_____

Billing Address_____Billing Zip + 4/Postal Code:_____

Signature:_____

WE ARE A NETWORK OF KNOWLEDGE

SMRT – A Global Community

The Section for Magnetic Resonance Technologists (SMRT) of the International Society for Magnetic Resonance in Medicine (ISMRM) is the leading non-profit organization that provides an international forum for education, information and research in magnetic resonance for technologists and radiographers throughout the world.

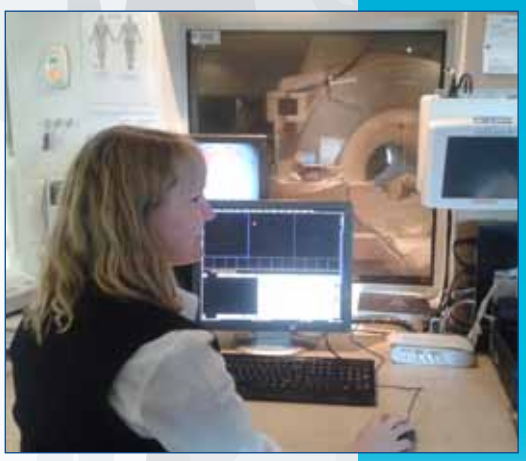

SMRT Member
Kate Negus, BaAppSci(RMIT)(MR)
MRI Supervisor
Barwon Medical Imaging
The Geelong Hospital
Geelong, Victoria, Australia

The SMRT was established by technologists, clinicians and scientists of the ISMRM as a forum for technologists and radiographers to share their expertise and educational resources, with a common goal of improving healthcare for people worldwide.

As an organization, we are committed to promoting communication and the dissemination of cutting-edge MR developments. The objective of the SMRT is to advance education and training, while striving to promote a high level of knowledge and professionalism in the field of MR technology and radiography.

SMRT

ISMRM
SECTION FOR MAGNETIC RESONANCE TECHNOLOGISTS

2030 ADDISON STREET
SUITE 700
BERKELEY, CALIFORNIA, 94704 USA
TEL: +1 510 841 1899
FAX: +1 510 841 2340
INFO@ISMRM.ORG/SMRT